Identification of Non-Coding RNAs Associated with Autism Spectrum Disorder and Cognitive Assessment of NMDA Receptor Modulators in Mouse

INAUGURALDISSERTATION

zur

Erlangung der Würde eines Doktors der Philosophie vorgelegt der

Philosophisch-Naturwissenschaftlichen Fakultät

der Universität Basel

von

Baran Koç

aus der Türkei

2019

Genehmigt von der Philosophisch-Naturwissenschaftlichen Fakultät auf Antrag von

Prof. Dr. Mihaela Zavolan

Dr. Benjamin J. Hall

Prof. Dr. Tania Rinaldi Barkat

Basel, den 23.04.2019

Prof. Dr. Martin Spiess

Dekan

To my grandparents Türkan and Beyhan

Acknowledgements

I wish to thank my advisor Dr. Benjamin Hall for his support and guidance throughout my research. His knowledge and teachings have provided me with the foundations to grow into a better scientist every day. I appreciate Dr. Eoin O'Connor for his support and providing the opportunity for exciting research collaborations. I would like to express my gratitude to my committee members Prof. Mihaela Zavolan and Prof. Tania Rinaldi Barkat for their invaluable time and efforts for my progress. I would like to extend my appreciation to Hall Lab members: Anja, Oliver, Jackie C., Eva, Imen, Michael, Jackie M., Joel, and to the "semi-member" Tev. I would like to thank all Ephys group members for their valuable comments and contributions. Especially Madhu for bringing her social and scientific enthusiasm to help me get through my PhD. Special thanks to Alex for being a great first lab mate at Roche. I truly appreciate Geoff for his invaluable contributions to our RNA-Seq study. A special acknowledgment to Ronald for helping us analyze RNA-Seq data and to Nicolas and Tobias for their scientific contributions. Thank you Roger for teaching me the finest tricks of animal experimentation. I would like to thank all the animal facility staff for their invaluable efforts. A big thank you to all my family and friends in Basel and beyond: Fabrizio, Alaz, Orçun, Mümün, İrem, Keith, Mehtap, Gizem İ., Nazlı, Ayşegül A., Seda, Maria Anna, Gizem Ö., Atılgan, Ayşegül B., Erhan, Bjorn, Benoit, Cristina, Clemens, Francesca, Mark and many more… I would like to express my greatest gratitude to my parents who supported me my whole life with their constant love and trust.

Table of Contents

Acknowledgements iv

Table of Contents v

Summary 1

Background 3

Autism Spectrum Disorder 3

Prefrontal Cortex 3

Striatum 4

Genetic and Molecular Underpinnings of ASD 5

Coding Genes Associated with ASD 5

NMDA Receptors 7

Cell-Specific Role of GluN2B-Containing NMDA Receptors 8

SynGAP 9

Long Non-Coding RNAs 10

General Characteristics of LncRNAs 11

Molecular Mechanisms of LncRNA Function 11

Involvement of LncRNAs in ASD 13

Targeting Natural Antisense Transcripts for Novel lncRNA-Based Therapies 14

Assessing Cognition in Animal Models 15

Working Memory 15

Trial Unique Non-Matching to Location (TUNL) Task 16

Pharmacological Studies with NMDA Receptor Modulators 16

Animal Studies 17

Results 20

Chapter 1 - Identification of Natural Antisense Transcripts in Mouse Brain and Their Association with Autism Spectrum Disorder Risk Genes 20

Abstract 20

Background 22

Methods 23

Results 28

Discussion 38

Supplementary Figures 45

Supplementary Materials 48

Chapter 2 - Diverse Modes of NMDA Receptor Antagonism Disrupt Working Memory by Affecting Different Behavioral Measures 49
Abstract 49
Introduction 50
Methods 52
Results 55
Discussion 63
Supplementary Figures 69
Supplementary Materials and Methods 79
Concluding Remarks and Future Outlook 81
References 83

Summary

Autism spectrum disorder (ASD) is a common neurodevelopmental condition characterized by impaired social interaction and communication as well as restricted and repetitive behaviors. The ASD etiology is complex and ill-understood. A combination of genetic and environmental factors is thought to be implicated in the ASD pathology. Many mutations have been linked to ASD in protein-coding genes. But long non-coding RNAs (lncRNAs) have attracted particular attention due to their role in the regulation of gene expression. In this thesis, I aimed to understand the transcriptional regulation of sense and antisense RNA transcripts related to ASD (Chapter 1), and to reveal the brain region-specific roles of GluN2B and Syngap1 in cognition (Chapter 2).

In Chapter 1, the primary focus was on 100 genes that were associated with ASD. Their sense and antisense transcript expression was profiled using a deep RNA sequencing approach. A small fraction of the examined transcripts showed brain region-specific enrichment in the medial prefrontal cortex (mPFC) or striatum across mouse development. Using this data, a *de novo* antisense transcriptome was generated with mPFC- and striatum-specific annotations, which yielded more than 70,000 antisense transcripts. A subset of these transcripts was validated in the mouse brain by qPCR. Moreover, the blast analysis revealed that a fraction of the *de novo* transcripts had high complementary coverage with the human genome.

In Chapter 2, the effects of NMDA receptor (NMDAR) antagonism on cognition were investigated. First, a touchscreen-based spatial working memory task for pharmacological testing was successfully optimized. Using this task, it was then demonstrated that the systemic administration of non-subunit selective uncompetitive antagonist MK-801 and

GluN2B-selective antagonist impaired working memory performance in mice by affecting different behavioral measures. Furthermore, by combining systemic NMDAR antagonism with genetic suppression of GluN2B or Syngap1 in mPFC, it was observed that loss of GluN2B exacerbated the MK-801-induced working memory impairment while Syngap1 knockdown animals showed reduced impairment.

Overall, the methods and results demonstrated in this thesis contribute to the understanding of the interplay of sense-antisense partners in the regulation of ASD-related genes and provide insight into how NMDARs and an associated cellular signaling molecule contribute to specific features of working memory. The results presented here could be used to define mechanistic targets in preclinical animal models with the ultimate goal of developing novel therapeutics for people in need.

Background

Autism Spectrum Disorder

Autism Spectrum Disorder (ASD) is a group of neurodevelopmental conditions that include abnormal social interactions, impaired communication as well as stereotypical and repetitive behaviors (1). Current estimation for ASD prevalence is 1 in 68 children, and significantly more common (1 in 42) among boys (2). ASD is heterogeneous and can arise from epigenetic, genetic and environmental factors (3). Disease can manifest itself with behavioral abnormalities, delayed language development, intellectual disability, epileptic encephalopathy, soft neurologic motor signs, and presence of non-neurologic conditions like gastrointestinal and cardiac complications (4-7). Various studies demonstrated that neurological and neurodevelopmental processes are disturbed in ASD, particularly establishment and maintenance of cortical excitatory/inhibitory balance (8), functional local versus long-range connectivity among cortical brain regions (9, 10), and increased number of neurons (11, 12). Dysfunction in several brains regions and neuroanatomical abnormalities have been associated with the pathology of ASD (13).

In this thesis, I focused on the transcriptional profiles of ASD-related genes and their associated antisense transcripts in medial prefrontal cortex (mPFC) and striatum, as well as mPFC-specific cognitive assessment of N-methyl-D-aspartic acid (NMDA) receptor modulation in mouse.

Prefrontal Cortex

The prefrontal cortex (PFC) is the execution hub of the human brain and it controls many higher-order cognitive processes including working memory, decision making, emotions, social behavior, communication and learning (13). Several functional and structural

changes have been identified in PFC of ASD brains. Neuroimaging studies have revealed overgrowth of prefrontal regions in autistic children. Moreover, abnormal functional asymmetry and activation between the cortex and cerebellum have been observed (14). Postmortem studies revealed autistic brains had 67% more neurons in the PFC and increased brain weight compared to neurotypical brains (11). PFC has been the main focus of many ASD studies due to its role in emotional processing and social communication which are disturbed in or individuals with ASD.

Striatum

The striatum is the critical regulator of motor and reward systems in the brain. It acts as a central relay station of inputs received from a number of cortical, thalamic and limbic brain regions to basal ganglia (15). Striatal circuits are proposed to be involved in behavioral flexibility, motivational state, goal-directed learning, and attention (16), which can be associated with ASD symptoms (Fig. 1). Striatal dysfunction is hypothesized to be responsible for the repetitive motor behavior present in ASD, and several imaging and neurological assessment studies supported this postulation (17) Given that multiple lines of evidence suggest that striatal dysfunction is associated with the core symptoms of autism including social and cognitive deficits, a more thorough understanding of its genetic makeup would be important to understand the underling physiology and define the mechanistic targets for ASD.

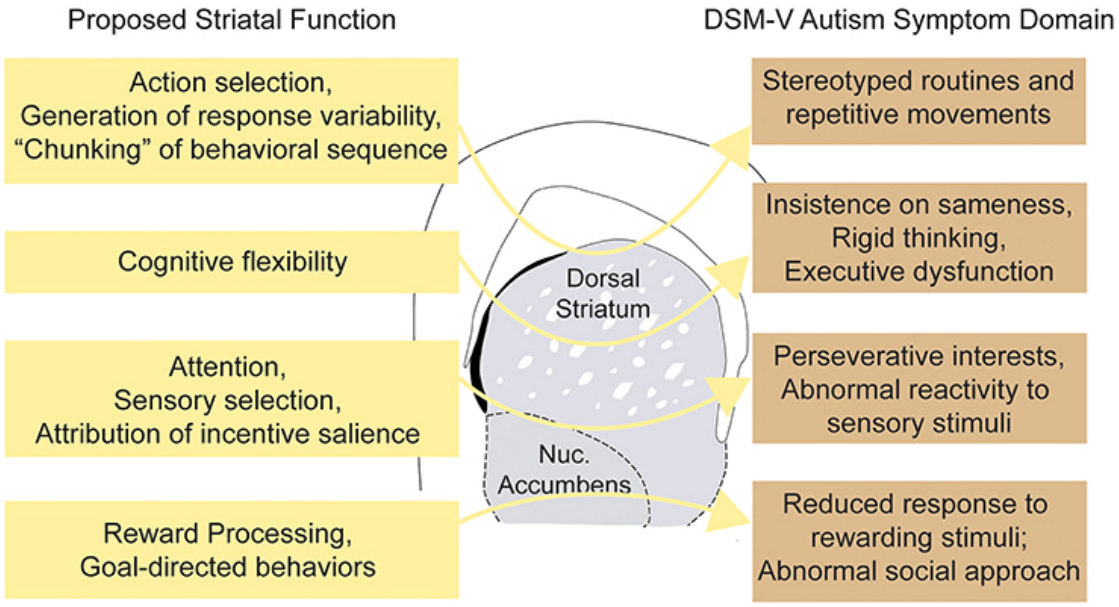

Figure 1. Proposed striatal functions and their association with autism symptom domains. Taken from Fuccillo et al. (17).

Genetic and Molecular Underpinnings of ASD

The definitive etiology of ASD remains unknown; it can arise from environmental, epigenetic and genetic factors. High concordance rates among monozygotic twins (18, 19) and increased autism recurrence among siblings (20) indicate a strong genetic component. The current estimation of ASD heritability is around 50% (21, 22). Besides heritability, there are also genetic factors that occur as *de novo* mutations with an estimated contribution of 15-20% to ASD etiology (23). Overall, genetic elements account for the highest portion of ASD risk factors. Studying the regulation of gene function and their molecular products would be informative for understanding the pathological mechanisms leading to ASD.

Coding Genes Associated with ASD

1,503 genes associated in ASD are listed by the most recent SFARI database, as of January 15, 2019 (https://www.sfari.org/resource/sfari-gene/) (24). Most of these ASD susceptibly

genes have been proposed to have various roles in neural development and neuronal function, including metabolism, synaptic transmission, RNA splicing and neuronal migration (25). Despite high genetic liability for ASD, the genetic architecture has various contributors (Fig. 2): "alleles of varying frequencies (i.e., common, rare, very rare), inheritance patterns (i.e. dominant, recessive, X-linked, de novo), and variant type (i.e., large chromosomal rearrangements, copy number variants (CNV), small insertions/deletions (indels), and single-nucleotide variants (SNVs)" (5).

Although it accounts for a small number of ASD cases, there are more than 100 rare Mendelian syndromes associated with ASD (24, 26) with a large effect size (21). Characteristic syndromes with ASD comorbidity and their associated genes are as follows: fragile X syndrome (*FMR1*), Rett syndrome (*MECP2*), tuberous sclerosis (*TSC1* and *TSC2*), Timothy syndrome (*CACNA1C*), and dup15q syndrome (5). On the other hand, CNVs account for the majority of cases with a small effect size. The studies from Simons Simplex Collection, which screened families of ASD individuals with unaffected siblings, demonstrated that ASD-associated CNVs (15q11.2–q13 duplications of the affected region in Prader-Willi and Angelman syndrome, 16p11.2 deletion, 16p11.2 duplication, and X-linked deletions including the PTCHD1-PTCHD1AS locus) are affecting cellular functions including neuronal development and axon guidance, synaptic signaling and function, as well as chromatin modification and transcription regulation (27, 28). *De novo* SNVs contributed significantly to the variety of ASD-associated genes thanks to the development in gene-hunting technologies and methods, especially with the emergence of whole-exome sequencing (29). Despite genetic heterogeneity, a converging pathophysiology is evident for most of the associated genes (25, 27, 30). For example, strongly implicated *de novo* SNVs have been identified in *SYNGAP1* and *GRIN2B* (coding for NMDA receptor subunit GluN2B) loci (Fig. 2), are implicated in the biologic processes involved in cognition (5) and part of

the glutamate receptor signaling pathway. In this thesis, we focus on the effects of NMDA receptor modulation on cognition by GluN2B and Syngap1-specific manipulations.

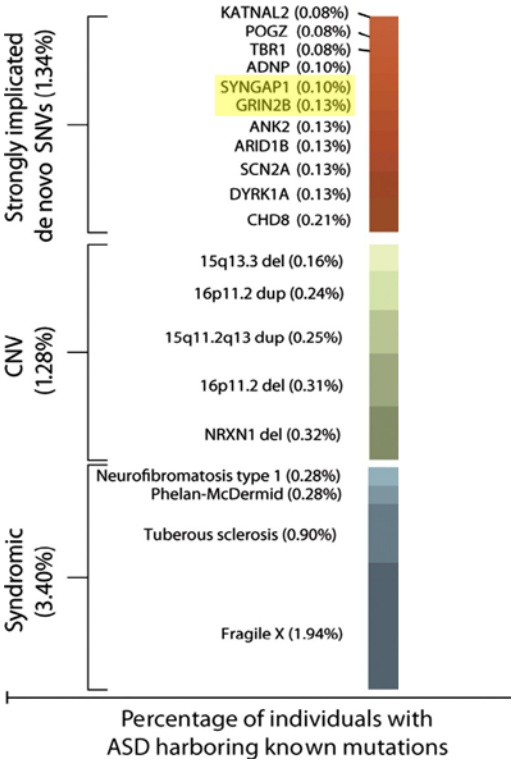

Figure 2. Genetic makeup of individuals with ASD. Modified from Ramaswami & Geschwind (2018).

NMDA Receptors

Glutamate is the main mediator of the majority of excitatory neurotransmission in CNS. It acts on various receptors including ionotropic glutamate receptors, which pass cations and are categorized under three families: α-amino-3-hydroxy-5-methyl-4-isoxazolepropionic acid (AMPA) receptors, kainite receptors, and NMDA receptors (NMDARs) (31). NMDARs are important mediators of synaptic plasticity with their function as coincidence detectors between pre and post-synaptic activities (32). They can convert specific patterns of neuronal activity into long term changes by structural and functional changes in synapses which are shown to be instrumental for cognitive functions (33)

Numerous NMDA receptor combinations can be assembled from one obligatory GluN1 subunit (encoded by 1 gene but alternatively spliced to 8 isoforms), four GluN2 subunits (GluN2A-D, encoded by four genes), and two GluN3 subunits (GluN3A and GluN3B, encoded by two genes). Heterogeneity in NMDARs can lead to functional diversity by affecting biophysical and pharmacological properties, interacting partners and subcellular localizations (33-35). Dimeric GluN1/GluN2A and trimeric Glu1/GluN2A/GluN2B receptors are the predominant receptor combinations present in the adult forebrain (36, 37).

Differences in GluN2 subunit have major consequences in the receptor properties (38-40). A key difference is the developmental regulation of subunit expression. GluN2A expression increases from birth to adulthood, while GluN2B expression starts high at birth, and decreases during brain development and remains primarily in the forebrain (41). Their channel kinetics also differ: GluN2A-containing NMDARs have a higher open probability and a faster decay than GluN2B-containing receptors, which are more sensitive to extracellular glutamate (33, 42, 43). Moreover, receptor subunit composition can be dynamic (44); GluN2A and GluN2B subunits can diffuse between synaptic and extrasynaptic sites (45). This mobility is important for the regulation of receptor number and subunit composition (33). Another difference comes from their signaling partners (46). GluN2B specifically interacts with downstream signaling molecules that regulate AMPAR trafficking and synthesis to maintain homeostatic plasticity.

Cell-Specific Role of GluN2B-Containing NMDA Receptors

GluN2B-contaning NMDARs provide unique properties to the synapses they are located through specific interactions with downstream intracellular signaling molecules in the postsynaptic density. During development, GluN2B-containing receptors link NMDAR activity to AMPARs by negatively regulating the AMPAR synthesis and trafficking in a protein synthesis-dependent manner (38, 47). Specificity of GluN2B-receptors is sustained

through their unique interaction with the calcium-dependent protein kinase CaMKII, which regulates the activity of other downstream postsynaptic density molecules including Syngap1, ERK, Rheb and mTOR (48-50). GluN2B reduction disinhibits mTOR-dependent translation of AMPAR and trafficking, hence increases excitatory synaptic strength, which is a critical feature of homeostatic synaptic plasticity (50). This critical role in excitatory synapse function is unique to GluN2B as replacement with GluN2A does not rescue phenotypes related to these cellular signaling processes (38).

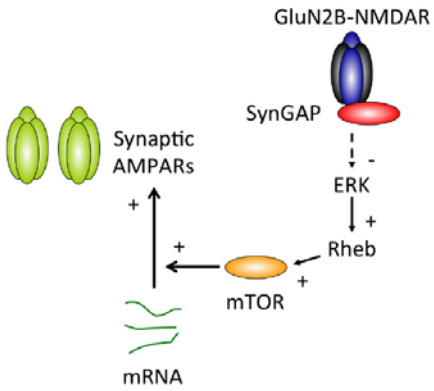

Figure 3. Proposed model of the GluN2B and SynGAP-mediated cellular signaling pathway. Taken from Wang et al (50).

SynGAP

Syngap1 (a.k.a. SynGAP) is a ~140 kDa, brain-enriched synaptic GTPase activating protein and is located exclusively at postsynaptic density of excitatory synapses (51, 52). It is a downstream component of the NMDA receptor signaling complex and negatively regulates Ras- and Rap-GTPases (53-55). SynGAP has a critical role in glutamatergic neurotransmission by regulating AMPA receptor synthesis and its trafficking to the membrane (56). SynGAP is selectively associated with GluN2B-containing NMDARs (57). Knocking down GluN2B or SynGAP *in vitro* leads to the disruption of translation-dependent homeostatic synaptic plasticity –indicating this pathway's role in maintaining

developmental synaptic plasticity (50). SynGAP also plays an important role in regulation of the dendritic spine formation and stability (56). SynGAP is therefore a major cell signaling protein that regulates fundamental changes in dendritic spine morphology and function in excitatory synaptic transmission (50, 58, 59).

SynGAP mutations have been highly associated with intellectual disability manifesting in early childhood where most cases are comorbid with encephalopathies (around 70%) and ASD (>50%) (60, 61). All identified SynGAP mutations cause loss-of-function and haploinsufficiency (62), meaning that the intact copy of the gene is not enough to compensate full physiological function.

Interestingly, a natural antisense transcript (NAT) for SynGAP (SynGAP-AS) has been identified in humans and increased antisense transcript expression was reported in ASD brain compared to healthy controls (63). This opens a possibility to endogenously enhancing SynGAP expression through SynGAP-AS interference. To date, no SynGAP-AS has been reported in mice or rats.

Long Non-Coding RNAs

International transcriptomics research consortiums like ENCODE (64-66), GENCODE (67, 68), and FANTOM (69, 70) showed that the human genome is widely transcribed and the main output is non-coding RNAs (ncRNAs). Although ncRNAs were once referred as “junk DNA” (71), it was later understood that ncRNAs can be functional by regulating developmental processes in various organisms (72, 73). A systemic categorization of ncRNAs have been made based on their length (short, medium, long) and their position with respect to protein-coding genes on the genome (intergenic, genic; sense, antisense) (68, 74).

General Characteristics of LncRNAs

In general, long non-coding RNAs are defined as transcripts that are longer than 200 nucleotides lacking an open reading frame with protein coding potential (75). Previous studies suggested that most lncRNAs share structural similarities with mRNAs such as polyadenylation, 5' cap and alternative splicing (70, 76, 77). They tend to be shorter than mRNAs and have lower number of exons (67, 78). Their expression levels can be greatly lower than protein-coding genes making them more difficult to identify and quantity (67, 79). Another interesting aspect of lncRNAs is that their sequences are less evolutionarily conserved compared to mRNAs (67). However, the promoter region of the lncRNAs are evolutionarily conserved and associated with transcription factor binding sites that give them their high tissue specificity (67, 80). LncRNAs have been shown in the mouse brain to be remarkably cell-type, region and tissue specific (81). This specificity feature has suggested that lncRNAs could have functional roles in neurodevelopmental processes, and possibly in cognitive development (74).

Molecular Mechanisms of LncRNA Function

A growing number of studies demonstrated that lncRNAs have various functional roles through interactions with DNA, RNA, and proteins (82) (**Fig. 3**). Depending on the cellular localization, they form various interactions with basic cellular molecules such base-pairing with short RNA stretches, acting as structural domains in the chromosome, and regulating allosteric transcription binding to DNA (82). At the transcriptional level, lncRNAs can act as RNA decoys and hinder the activity of transcription factors to bind their DNA-binding motifs (82, 83). By doing so, they can interfere with alternative splicing events. Another role of lncRNAs is that they can act like microRNA "sponges" and reduce the activity of microRNAs (miRNAs) to associate with their target mRNAs (82, 84, 85). In this way, the reduced activity of miRNA can lead to the disinhibition of mRNA degradation, therefore,

upregulation of the mRNA levels. This titration effect has also been shown to affect other molecular targets such as transcription factors (85). Many lncRNAs have been demonstrated to bind to regulatory protein complexes to act as scaffolding elements to bring protein molecules into physical proximity, such as in the ribonucleoprotein (RNP) component (86, 87). Besides, they can have *cis* regulatory effects on the DNA that causes the recruitment of chromatin modifiers and affect genes from distant genomic regions (86). These protein modifying complexes are particularly important during development as they can modify the expression environment by activating or silencing genes (82). Also, lncRNAs can bind directly to mRNA to interfere with their expression by inhibiting translation, modulating splicing, and triggering degradation (88, 89). Overall, lncRNAs have important gene regulatory roles in developmental processes by affecting transcription and translation (82).

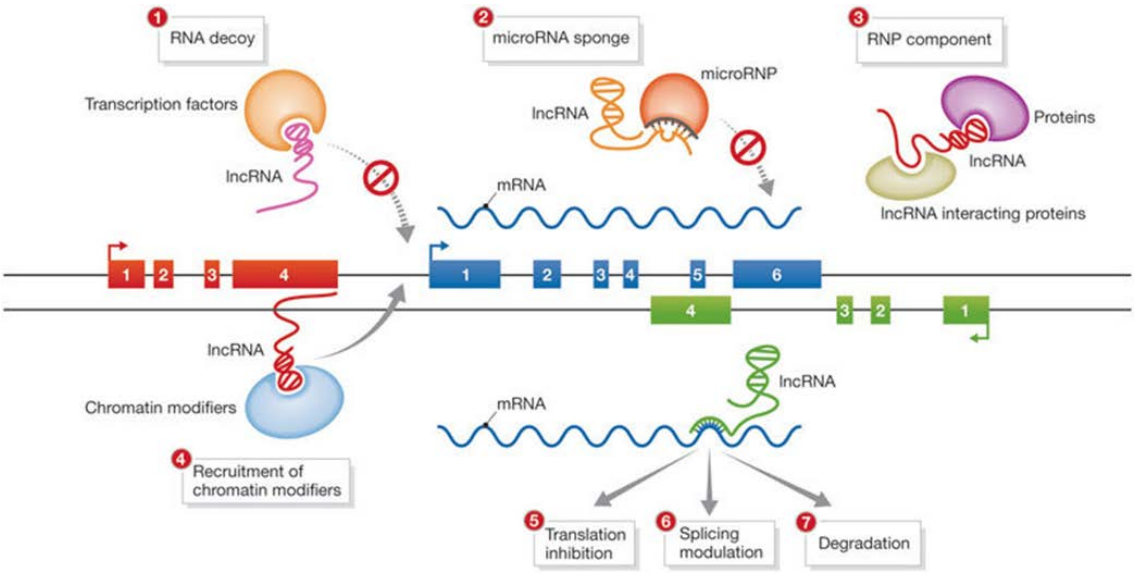

Figure 4. Overview of the molecular mechanisms of lncRNA function. lncRNAs can regulate gene expression through different mechanisms: **(1)** Titrating transcription factors away

from their DNA targets as RNA decoys, **(2)** Acting as microRNA sponge to titrate miRNA complexes away from their mRNA targets, **(3)** Acting as scaffold elements within ribonucleoprotein complexes, **(4)** Recruitment of chromatin modifying complexes. Moreover, their mRNA regulatory roles include: **(5)** translational inhibition, **(6)** splicing modulation, and **(7)** degradation. Taken from (82).

Involvement of LncRNAs in ASD

It has been suggested that the diversity of non-coding elements and the complexity of organisms are correlated (73, 90). For example, the lncRNAs present in the PFC of macaque monkeys and humans have been reported to have spatiotemporal expression profiles and conserved in a similar way to the protein-coding genes between two species (72, 90, 91). This finding has suggested that lncRNAs could play important roles in cognitive processes and neural development (72, 92). Moreover, previous studies have reported that lncRNAs were involved in neuronal variation and specification (72). Therefore, it is a great possibility that lncRNAs could be related to pathological events in the brain due to their roles in transcriptomic regulation, and neurodevelopmental diseases such as autism.

In fact, there are a number of studies proposing a possible link between aberrant lncRNA expression and ASD (93). Using a bioinformatics approach, Velmeshev et al. examined the publicly available transcriptomics database Aceview and identified non-coding antisense (AS) RNA transcripts in genomic regions related to ASD (63). Moreover, they confirmed the expression of 10 ASD-related AS transcripts in postmortem human brain tissue by qPCR. They also demonstrate that *Syngap1*/*Syngap1*-AS pair had a discordant expression pattern and *Syngap1*-AS was upregulated in the PFC and temporal gyrus of ASD brains compared to non-ASD controls. In a genome-wide transcriptome analysis using RNA-Seq, ASD-related differential expression of 60 primate-specific, brain-enriched lncRNAs in post-mortem brain tissue (frontal and temporal cortices and cerebellum) was reported (94). These lncRNAs

had little functional annotations and 20 of them were shown to interact with miRNA complexes and 9 of them with the ASD-related fragile X mental retardation protein (FMRP). In a microarray profiling study, 222 out of 33,000 lncRNAs in PFC and cerebellum were found to be differentially expressed between ASD and control brains (95). Also, GWAS have identified a strong association with ASD for a single nucleotide polymorphism in the region where the lncRNA *MSNP1*-AS was transcribed (96). Overall, these studies provided a new angle for the functional roles of lncRNAs in the brain and their association with ASD.

Targeting Natural Antisense Transcripts for Novel lncRNA-Based Therapies

Conventional drug discovery research has been mainly concentrated on regulating the activity of proteins, which is encoded by 2% of the genome (74). On the other hand, 80% of the genome is transcribed into RNAs, which makes them a big potential as drug targets with a great temporal and spatial specificity (74). There is a particular interest in developing genomic medicine for CNS disorders due to their low systemic exposure and toxicity, extended half-life as well as their versatile potentials to regulate gene expression up or down and modify splice editing, that are not typically feasible with traditional small molecule modalities or biotherapeutics (97, 98).

Natural antisense transcripts (NATs) are a class of lncRNAs encoded from the opposite strand of a protein-coding gene locus (99). They can regulate the expression of protein coding genes in *cis* (99). They demonstrate a high degree of target specificity due to their complementary sequences (100). Single-stranded oligonucleotides can be used to inhibit their function and thereby upregulate the expression of their target protein coding genes (69, 74, 101). These oligonucleotides are called *antagoNATs* and they have been successfully tested *in vitro* and *in vivo* (74, 102). Absence of nucleases in the cerebral spinal fluid makes them a promising approach to be used in neurological disorders (74).

Assessing Cognition in Animal Models

Cognitive disturbances are a common symptom in many neurodevelopmental disorders including ASD (103-106). Despite cognitive impairment is recognized as a key target to reduce and prevent psychiatric impairment, treatment opportunities are still limited (107). There is plenty of research that implements behavioral paradigms in animal models and demonstrate efficacy of cognitive enhancers for neurodevelopmental disorders (107). In clinical studies, these targets cannot show the predicted efficacy in animal models and fail in translatability (108). Therefore, having a mechanistic understanding of how therapeutics work is an important virtue for developing and polishing new molecules.

Touchscreen cognitive testing methods have been developed to overcome the mismatch between how cognitive functions are assessed in animal models and humans allowing to assist inter-task associations and reduce confounds (107, 109-111). The Trial-Unique Non-Matching to Location (TUNL) is a touchscreen-based task developed to test working memory domain of cognition in rodents (112, 113).

Working Memory

Working memory is the ability to retain information that is no longer explicitly present to execute a cognitive task or make a decision (114). Persistent neural activity in the prefrontal cortex has been linked as the neural correlate of working memory (115, 116). For rodents, working memory can be defined as “a short tem memory for an object, stimulus, or location that is used within a testing session, but not typically between sessions” (117). Several working memory tasks have been developed for rodents: maze tasks such as delayed alternation, radial arm, Morris water maze; delayed non-matching to sample with objects or samples, and operant tasks including TUNL (117).

Trial Unique Non-Matching to Location (TUNL) Task

The TUNL task is used to assess spatial working memory in rodents and can be translatable to humans (112, 118). In TUNL, an automated operant chamber allows working memory assessment by requiring the animal to choose a nonmatching location after a variable delay following a sample phase to receive a food reward upon successful completion of the trial. The TUNL task can be divided into several quantifiable components. In this way, detailed assessment of working memory is possible due to precise measurement of task parameters such as response latencies (113).

TUNL task offers many advantages including being automated, non-aversive and low-stress, having the ability to assess multiple cognitive domains and being translational across species (118). It offers a various neuropsychological constructs such as attention and cognitive flexibility, and it uses appetitive motivation, rather than aversion (119). The task has been shown to be sensitive to hippocampus and cortex dysfunction (112, 120, 121). A disadvantage of TUNL is that it might take more than several weeks for animals to learn the task; however, specific modifications can be applied to make the task more rapidly-acquired (118).

Pharmacological Studies with NMDA Receptor Modulators

A multitude of pharmacological studies has been conducted in animal models and humans to understand cognition, and glutamatergic modulation has been in the focus of these efforts (122). Here, the pharmacological experiments are highlighted in relation to their use of NMDAR modulation.

Acute NMDAR antagonism with ketamine, phencyclidine and dizocilpine has been shown to have a negative effect on cognitive function in rodents such as cognitive flexibility and attentional processing (122-127). Impairment cause by acute NMDAR antagonism has been also observed in other cognitive domains including spatial learning and memory, object

recognition memory, associative memory, and episodic memory and learning (122). Motivational and motor deficits have also been observed after acute NMDAR antagonism and this feature can possibly confound with other cognitive measures (128) However, these drawbacks can be eliminated by arranging dose or time of administration (122). Another drawback is that these compounds might not only selective for NMDARs, and can display off-target effects for example in the case of ketamine (128). Therefore, implementing genetic studies is important to test the effect of NMDAR modulation on cognition.

The assessment of NMDAR antagonism's effects on working memory in TUNL has been mainly performed in rats. Systemic injection of antagonists MK-801 and CPP impaired working memory performance while GluN2A-specific antagonist NVP-AAM077 or GluN2B-selective antagonists CP 101-606 or RO 25-6981 did not show any significant effect on test accuracy (129, 130). Injection of the competitive antagonist AP5 into mPFC and striatum also impaired the task performance in rats. Sodium nitroprusside (SNP), which is an adjunct treatment to reduce the working memory impairments experienced by schizophrenia patients, failed to block the detrimental effect of MK-801 in TUNL (130).

Animal Studies

NMDAR antagonist rodent models are widely used to study cognitive function and pathology (Fig. 5) (131). There are several studies specifically looked at the differences of NMDAR subunit composition and its effect on cognition in genetic mouse models (122). Here, GluN2B and Syngap1 genetic models will be summarized.

GluN2B knockout in principal neurons of the postnatal forebrain impaired spatial working memory, spatial reference memory, impaired recognition memory in a variety of behavioral tasks, and caused performance deficits in simple Morris Water maze and visual discrimination tasks (132). In the same study, it was also demonstrated that GluN2B knockout in hippocampus impaired spatial working memory and reversal learning;

however, no impairment in spatial reference memory was observed. Brigman et al. demonstrated that corticostriatal or striatal GluN2B removal, or dorsal striatum-restricted GluN2B antagonism impaired choice learning, while cortical Glu2B removal or orbitofrontal GluN2B antagonism caused an impairment in shift choice behavior (133). The same group also demonstrated that GluN2B removal in CA1 hippocampus and cortex disrupts a variety of behavioral tasks including Morris water maze, T-maze spontaneous alteration and fear conditioning in addition to reduced dendritic spine density. A recent study reported impaired cognitive flexibility following genetic GluN2B deletion in CaMKII-positive cell population (134). This study convincingly demonstrated that GluN2B deletion disrupted the coordination between orbitofrontal cortex and dorsal striatum by altering the neuronal firing rates that are necessary for optimal behavioral flexibility. In a homozygous 2B → 2A mouse model, social exploratory behavior was depressed and 2B → 2A mice spent less time exploring the novel mouse compared to wild-type controls in a social approach assay (38). Miller et al. showed that specific deletion of GluN2B in the excitatory cell population of mPFC caused a dramatic decrease in despair-like behavior compared to littermate controls in forced swim task and tail suspension task (135). The studies explained above and many others suggest that GluN2B-containing NMDARs are greatly involved in cognition related behaviors in rodents.

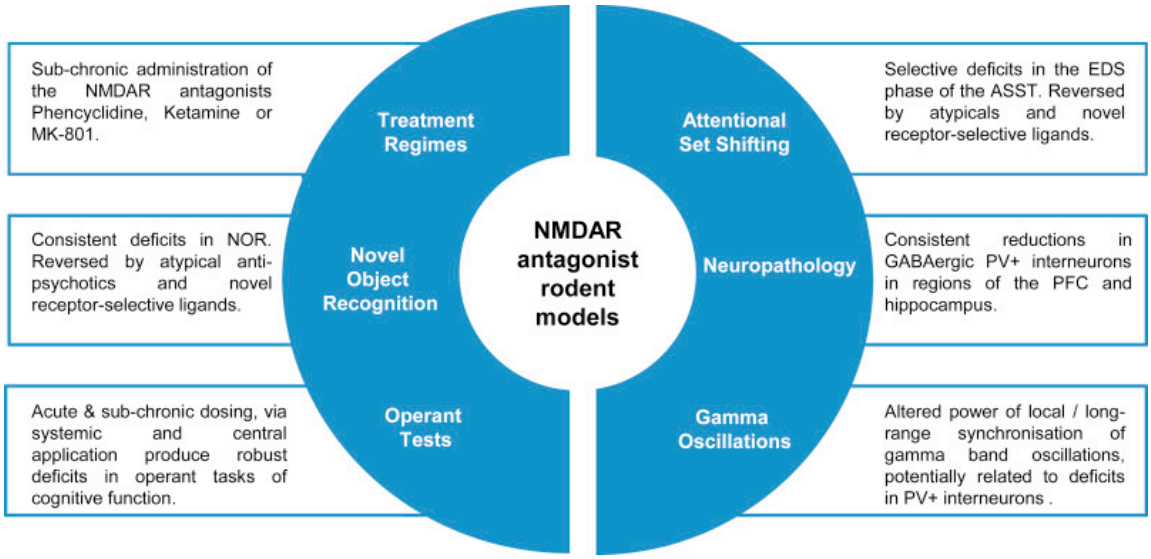

Figure 5. NMDAR antagonist rodent models are widely utilized for studying cognitive and pathological deficits. Abbreviations: NOR, novel object recognition; EDS, extra-dimensional shift; ASST, attentional set shifting task; PV+, parvalbumin positive; PFC, prefrontal cortex. Taken from Cadinu et al. (131).

Various studies have linked Syngap1-haploinsufficienct with behavioral deficits. One of the most common deficits in Syngap1$^{+/-}$ mice is hyperactivity (58, 136-140). Reduced levels of anxiety in Syngap1$^{+/-}$ mice was observed as increased exploration time in the open arm of the elevated plus maze and increased exploration time in the center area of an open field test (58, 136, 138, 140, 141). Syngap1$^{+/-}$ mice also demonstrate impaired learning in the Morris water maze (142). In other experiments, Syngap1$^{+/-}$ mice showed working memory deficits in spontaneous alternation test and in radial arm maze experiments (138, 143). Moreover, Syngap1$^{+/-}$ mice showed social function deficits such that they spent less time to explore a stranger mouse compared to wild-type controls (136, 140). Furthermore, Syngap1$^{+/-}$ mice have widespread and frequent cortical epileptiform discharges on EEG and a reduced threshold compared to wild-type mice (58, 141). Behavioral and physiological disturbances observed in SynGAP animals demonstrated that SynGAP is strongly involved in cognitive function in rodents.

Results

Chapter 1 - Identification of Natural Antisense Transcripts in Mouse Brain and Their Association with Autism Spectrum Disorder Risk Genes

Baran Koç[1, 2*], Geoffrey Fucile[3], Roland Schmucki[2**], Nicolas Giroud[2**], Tobias Bergauer[2**], Benjamin J. Hall[2*]

1- Faculty of Science, University of Basel, 4056 Basel, Switzerland

2- Pharma Research and Early Development, *Neuroscience Discovery, **Pharmaceutical Sciences, Roche Innovation Center Basel, 4070 Basel, Switzerland

3- sciCORE Computing Center, University of Basel, 4056 Basel, Switzerland

Correspondence to Benjamin J. Hall (benjamin.hall@roche.com).

Abstract

Background

Genome-wide sequencing technologies have greatly contributed to our understanding of the genetic basis of neurodevelopmental disorders such as Autism Spectrum Disorder (ASD). Interestingly, a number of ASD-related genes express natural antisense transcripts (NATs). In some cases, these NATs have been shown to play a regulatory role in sense strand gene expression and thus contribute to brain function. However, a comprehensive study examining the transcriptional relationship between ASD-related genes and their NAT partners is lacking.

Methods

We performed strand-specific, deep RNA sequencing to profile expression of sense and antisense reads with a focus on 100 ASD-related genes in medial prefrontal cortex (mPFC) and striatum across mouse development (P7, P14 and P56). Using *de novo* transcriptome assembly, we generated a comprehensive long non-coding RNA (lncRNA) transcriptome. We conducted blast analysis to compare the resultant transcripts with the human genome and identified transcripts with high sequence complementarity and coverage.

Results

Our analyses revealed that more than half of the examined ASD-related genes had strong antisense read expression; suggesting more ASD-related genes than previously thought could be subject to NAT-mediated regulation in mice. We found that expression levels of antisense reads were mostly negatively correlated with their coding sense strand RNA transcripts (~20%, $r<-0.90$). A small fraction of the examined reads showed brain region specific enrichment, indicating possible circuit-specific roles. We assembled over 70,000 *de novo* antisense transcripts and validated the expression of a subset of selected ASD-related transcripts by qPCR. Our blast analysis revealed a fraction of the assembled *de novo* transcripts were >90% complementary to the human genome with >90% coverage.

Conclusion

These findings, which include an assembled *de novo* antisense transcriptome contribute to the understanding of NAT regulation of ASD-related genes in mice by guiding NAT-mediated gene regulation strategies in preclinical investigations toward the ultimate goal of developing novel therapeutic targets for ASD.

Keywords

Natural Antisense Transcript, NATs, Autism, ASD, lncRNA, Development, mPFC, Striatum, Antisense Transcriptome

Background

Autism spectrum disorder (ASD) is a complex neurodevelopmental condition that manifests itself in early childhood with social interaction deficits, impaired communication and behavioral disturbances such as stereotypy and excess repetition (1). ASD is currently estimated to affect 1 in 68 individuals (144). Disturbances in frontal cortex, amygdala and cerebellum have been associated with autism after imaging or postmortem studies of ASD patients (145). While pathological changes in mPFC function likely contributes to impaired social behavior and communication, striatal circuit deficits likely underlie the repetitive and stereotypical behaviors (17). Both environmental and genetic factors can contribute to ASD (3). With recent advancements in genome-wide sequencing technologies, an increasing number of protein coding gene alterations have been linked to ASD (22). However, whole genome sequencing of samples from ASD families have identified potentially disease-relevant, non-coding RNA (ncRNA) variants in the human genome (5).

Non-protein coding DNA regions can be transcribed into two main ncRNA classes based on their nucleotide length: small ncRNA (<200 bp) and long ncRNAs (≥200 bp) (146, 147). Between 10 and 50 kbp long ncRNAs (lncRNAs) have been annotated so far in the human genome and a significant portion of these genes (40%) show brain-specific expression (67, 148). Natural antisense transcripts (NATs) are a specific class of lncRNAs and are synthesized from the DNA strand opposite from protein coding genes, with which they have sequence complementarity (69, 149). NATs can up or down regulate the expression of their sense mRNA partners by affecting *cis* or *trans* regulatory elements (63, 150). Many lncRNAs have been proposed to have important roles in brain development and their dysregulation

in neurodevelopmental disorders including ASD (63, 74, 90, 146, 151-158). Studying NATs in animal models allows testing of their biological function as well as developing and testing therapeutics that aim to modulate gene expression.

Here, we used a deep RNA sequencing approach to profile sense and antisense reads with a focus on 100 ASD-related genes in the mPFC and striatum across mouse development. Using these data, we built a *de novo* antisense transcriptome and then used this to identify antisense transcripts in mouse that are highly complementary with the human genome. The information provided here can guide efforts to test NAT-mediated regulation of ASD genes.

Methods

Animals and Tissue Preparation

Experiments were conducted in adherence to the Swiss federal ordinance on animal protection and approved by the Canton of Basel Stadt Veterinary Authority. Wild-type mice were from C57BL/6 background and obtained from Janvier Labs (Le Genest-Saint-Isle, France). Brains were removed at three different postnatal ages (P7, P14, and P56). There were 2, 5, and 5 animals from P7, P14, and P56 groups, respectively. Following removal, brains were immediately cooled in ice-cold HBSS (See Supplementary Materials and Methods). Each brain hemisphere was transferred into cold RNAlater stabilization solution and kept at 4°C for 24 hours, and transferred to -20°C until sample collection for RNA isolation.

On the day of RNA isolation, samples were thawed on ice. Each brain sample was manually sliced at room temperature into approximately 1 mm-thick coronal sections. Anatomical locations of mPFC and striatum were determined under stereo microscope according to a published protocol (159). mPFC or striatum samples were collected from brain slices using

a tissue punch, 2 mm diameter for P14 and P56 animals, and 1.5 mm in diameter for P7 animals. Striatal samples were a mixture of dorsal and ventral regions.

RNA Sequencing and Quality Control

Total RNA including miRNA fractions were isolated using Qiagen miRNeasy mini kit according to the manufacturer's protocol. RNA integrity was assessed with an Agilent 2100 Bioanalyzer using an Agilent Bioanalyzer 6000 Nano kit. Input of 400ng of total RNA was used as starting material for each sample and libraries were prepared using TruSeq Stranded Total RNA LT with Ribo-Zero Gold Depletion Kit from Illumina. Quantification was performed using KAPA Library Quantification Kit and the average size of 300 bp was determined by using a High Sensitivity DNA Kit. The libraries were pooled and diluted to 13 pM to load on an Illumina HiSeq 2500 Instrument.

RNA-Seq paired-end reads of 24 mouse brain samples were mapped onto the mouse genome (mm10) using the short read aligner GSNAP with default parameters (160, 161). The number of mapped reads for all mouse RefSeq transcript variants of a gene (counts) were combined into a single value using SAMtools software (162) and normalized to RPKMs (number of mapped reads per kilobase transcript per million sequenced reads) (163).

Multidimensional scaling was used to plot individual samples and illustrate the global landscape in terms of inter-relation of samples (distance). Pair-wise correlation analysis was performed to reveal similarity of the samples. As a quality control, we determined the fraction of reads per sample mapped to ribosomal transcripts. In one of the samples this fraction was higher than 10% and therefore the sample was discarded for further downstream analysis. Aligned reads were separated into forward and reverse mapped reads using SAMtools software (162) (see additional material for BAM files).

Identifying Antisense Reads for ASD-Related Genes and Correlation with Sense Reads

We adopted a list of 103 ASD-related genes from a previously published study which used a bioinformatics pipeline to identify NATs in genomic regions related to ASD (26, 63). We screened mouse orthologues of these genes on Ensemble (Release 90) and found that 100 of these genes have a 1-1 mouse orthologue (*NLGN4X*, *ZNF674*, and *ZNF81* were the exceptions) (See additional material for complete gene list). We used these 100 ASD-related genes in our analyses unless otherwise stated.

The coding locus of each ASD-related gene was extended on both 5'- and 3'-prime ends by including 5 kbp flanking regions. This extended locus was compared to other known gene loci on the reverse strand to determine overlapping regions. Overlaps were removed from the locus with a 50 bp buffer, yielding an overlap free zone. Uniquely aligned reads within overlap free zone were determined (grey blocks in Fig. 3A). We quantified the abundance of antisense reads by calculating their relative ratio relative to total reads (sense + antisense reads), which we named *antisense read score*.

We analyzed the correlation of sense and antisense reads over our three developmental ages. We averaged the expression values of antisense and sense reads at P7, P14, and P56 and then used the Pearson correlation coefficient to assess the correlation between sense and antisense reads. A correlation coefficient +1 would indicate a perfect positive linear correlation, while -1 would indicate a perfect negative linear correlation.

Differential Expression Profiling of Antisense Reads Around ASD-Related Genes and Across Brain Regions

For expression profiling of antisense reads, we developed a simple formula that demonstrates the relative abundance of antisense reads across two brain regions, mPFC and

striatum. Where a positive Differential Expression Score (DES) specifies greater abundance of mPFC reads, and a negative DES would indicate increased relative abundance in striatum.

$$\text{Differential Expression Score (DES)} = 100\, x \frac{\left(\frac{mPFC_{Opp_{Reads}}}{mPFC_{Total}}\right) - \left(\frac{Str_{Opp_{Reads}}}{Str_{Total}}\right)}{\left(\frac{mPFC_{Opp_{Reads}} + Str_{Opp_{Reads}}}{Total\ Reads}\right)}$$

De Novo Antisense Transcriptome Assembly

Reads which mapped in antisense orientation to genomic features (i.e. genes) were used to create a *de novo* antisense transcriptome. Reads were aligned against mouse genome reference (GRCm38) using STAR (164). Binary alignment maps were categorized as sense and antisense reads. *De novo* transcriptome assembly using the Trinity platform (165, 166) was applied to mPFC and striatum samples separately and contiguous sequences (a.k.a. *contigs*) were obtained. Identical and enclosed contigs were determined and repetitive contigs were removed. Remaining contigs were masked for overlapping features and blasted for verification. Raw reads were then re-mapped to these contigs, and counts were summarized by contig. Differential expression analysis was conducted using both DESeq2 (167) and edgeR (168, 169) methods, contrasting both age and niche as well as full models. Contigs might map to more than one gene and/or a single gene might have multiple contigs mapped against it. We used contigs to determine putative natural antisense transcripts. Appropriate statistical tests were used to determine significance of differentially expressed contigs.

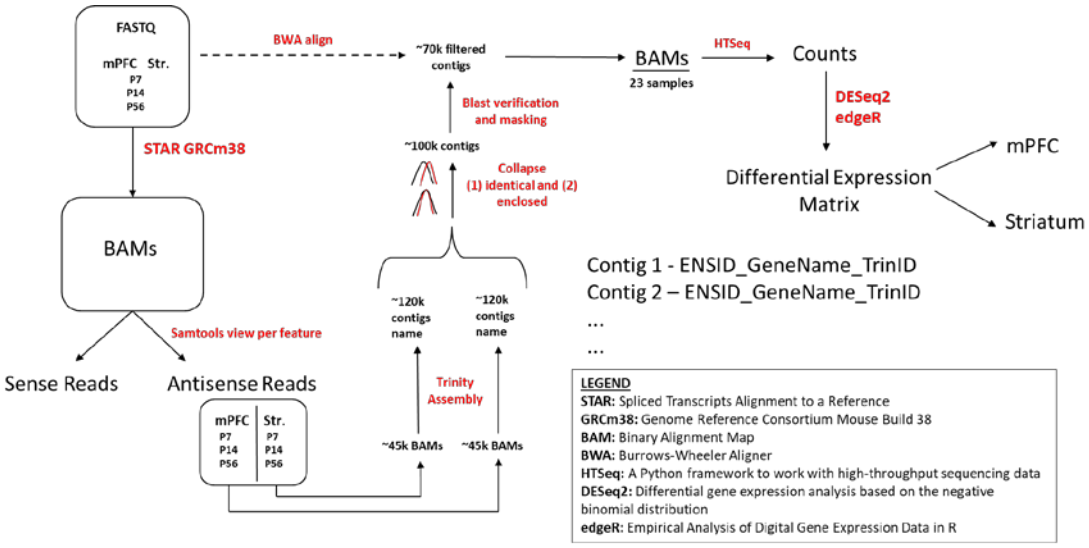

Figure 1. Bioinformatics pipeline used for *de novo* antisense transcriptome assembly.

Determination of Putative NATs with High Human Complementarity

Putative NATs from mouse which mapped as antisense to the human genome were determined by blast analysis. The criteria for high complementarity between mouse and human were set as >90% coverage and >90% identity.

RT-qPCR for Assessing Putative NAT Expression

One-step RT-qPCR was performed using AgPath-ID™ One-Step RT-PCR kit (Cat# 4387391, Thermo Fisher Scientific) according to the recommended protocol with a Roche LightCycler® 480 Instrument (Roche Molecular Systems, Inc., Pleasanton, CA, USA). Pre-designed and custom-designed TaqMan probes (Thermo Fisher Scientific) were used (see Supplementary Materials and Methods for TaqMan probe sequences). C_t values were calculated using absolute quantification/2nd derivative maximum method in high confidence mode with LightCycler® 480 Software, Version 1.5.

Results

Profiling ASD-Related Genes in mPFC and Striatum across Development Revealed Differentially Expressed Sense Strand Reads

Brain region-specific expression of genes can give insight about their function in disease relevant brain regions. Thus, we first aimed to identify genes preferentially expressed in either mPFC or striatum –two brain regions implicated in ASD. For this analysis, we ranked genes based on their average, normalized read counts, combined for all developmental time points and used these values as a proxy for their expression levels (Fig. 2A and 2B) (see Supplemental Table 1 for relative expression values). While most ASD-related genes we examined had comparable expression levels (Figure 2A), there was a fraction of genes that were differentially expressed (Figure 2B): *Satb2*, *Prss12*, *Mef2c*, *Nfix*, *Syn1* are enriched in mPFC; and *Foxp1*, *Ap1s2*, *Gamt*, *Igf2*, *Gucy2d* are enriched in striatum.

ASD is a neurodevelopmental disorder; therefore, understanding how ASD-related genes are regulated over development is important for understanding their function in synaptic development and circuit formation. To understand their developmental regulation, we ranked ASD-related genes by average expression across three developmental time points: P7, P14 and P56 (combined for both mPFC and striatum). These developmental time points overlap with transcriptomic changes related to synaptogenesis and synaptic maturation in mouse (170) and correspond to various stages of human brain development spanning from childhood to mature adult (171). To our surprise, most of the genes we examined did not show a strong developmentally-regulated expression profile (Figure 2C). The most strongly developmentally downregulated genes were *Dcx*, *Agtr2*, *C77370*, *L1cam*, and *Dhcr7*, while the most strongly upregulated genes were *Gria3*, *Iqsec2*, *Map2k1*, *Syn1*, *Slc6a8* (Fig. 2D).

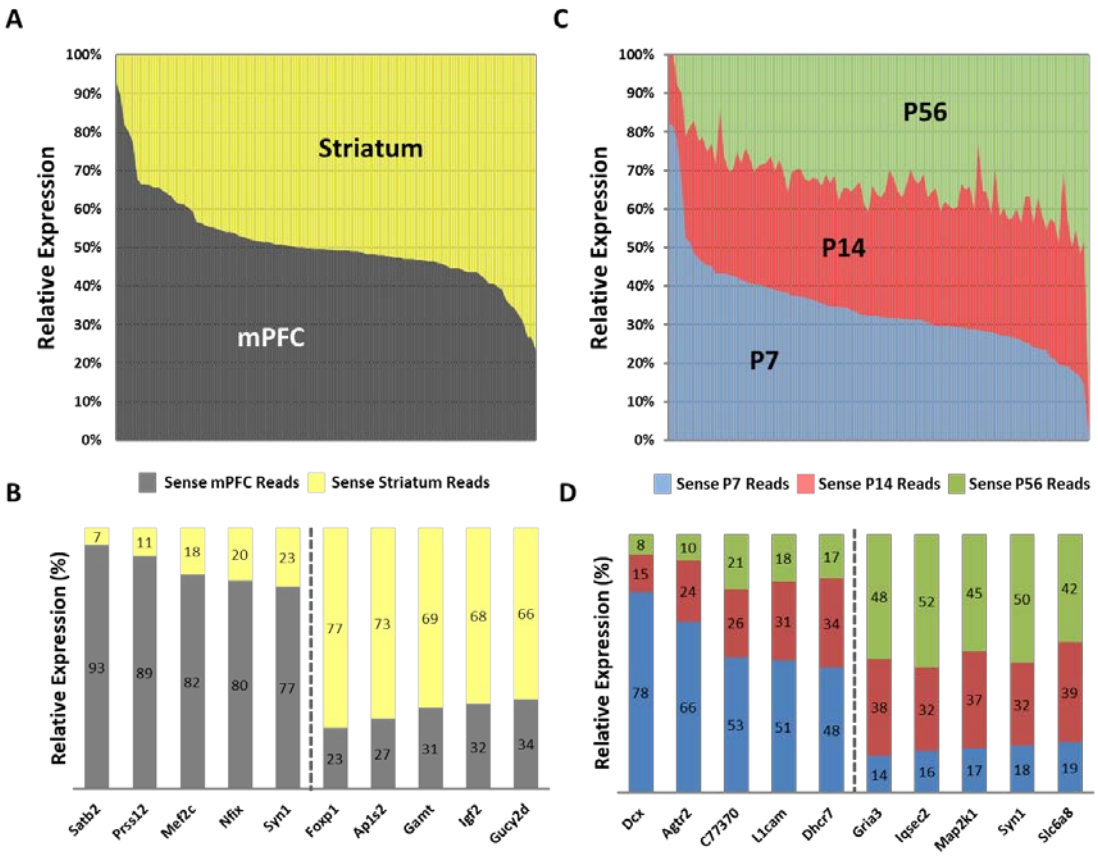

Figure 2. Sense strand read count profile of 100 ASD-related genes across brain regions and development.

A. Overview of ASD-related genes sorted based on their relative expression levels between mPFC and striatum (all ages combined). X-axis represents 100 genes; Y-axis represents relative expression. **B.** Five highly enriched genes for mPFC (left) and striatum (right). **C.** Overview of the ASD-related genes sorted based on their relative expression levels through development (P7, P14, P56) (all brain regions combined) X-axis represents 100 genes; Y-axis represents relative expression. **D.** Five developmentally downregulated (left) and upregulated genes (right).

Subset of Antisense Reads Showed Differential Expression in mPFC or Striatum

Natural antisense transcripts are mainly localized on the opposite strand of their partner coding genes and can overlap with UTRs, promoters, enhancers, introns, exons and flanking sequences (99). To maximize the probability of detecting non-coding transcripts, we analyzed antisense reads in the opposite strand of ASD-related genes and their 5k bp flanking regions (Fig. 3A). In the case where a coding genomic element overlapped on the opposite strand, we removed this section from our analysis while also including the corresponding 50 bp flanking regions. We then qualitatively grouped the antisense reads into three categories based upon their abundance relative to sense reads: strong antisense reads (42%), moderate antisense reads (17%), and weak antisense reads (41%) (Fig S1). Moreover, we classified these reads by whether or not they have any reported antisense transcripts in humans or cynomolgus macaques using the Aceview Transcriptome Database (172). The genes with reported macaque and human NATs and strong antisense reads in mouse are *Braf*, *Cacna1c*, *Foxp1*, *Nf1*, *Pafah1b1*, *Ube3a*, *Vps13b*.

We first analyzed the relative abundance of antisense reads compared to sense reads around ASD-related genes. By these terms, *Otc* showed the most abundant antisense reads (91.34%). *Cacna1f*, *Gucy2d*, *Ube3a* also had more antisense reads compared to sense reads. Antisense read scores for other genes were significantly lower compared to their sense counterparts (see table Table 1 for 10 genes with highest antisense read score).

Table 1. 10 ASD-Related Genes with Highest Antisense Read Score

Gene	Antisense Read Score
Otc	91.34
Cacna1f	88.43
Gucy2d	61.35
Ube3a	59.87
Hoxa1	32.93
Pah	17.39
Aldh5a1	14.44
Prss12	14.17
Mid1	9.71
Il1rapl1	5.67

Next, we quantified the differential expression of antisense reads in mPFC and striatum, which might suggest a brain specific regulation. We developed a simple measure (differential expression score) that takes into account the weight of opposite strand reads in mPFC or striatum within the total fraction of antisense reads. Our analyses revealed that only a small fraction of antisense reads displayed mPFC or striatum enrichment (Figure 3B). The 5 genes with the most mPFC-enriched antisense expression are *Rpe65*, *Agtr2*, *Ap1s2*, *Gamt* and *Mkks* (Fig. 3C), while the 5 top genes with striatum-enriched antisense expression are *Prss12*, *Mef2c*, *Rpgrip1l*, *Syn1* and *Kras* (Fig. 3D). For the complete list, see additional files.

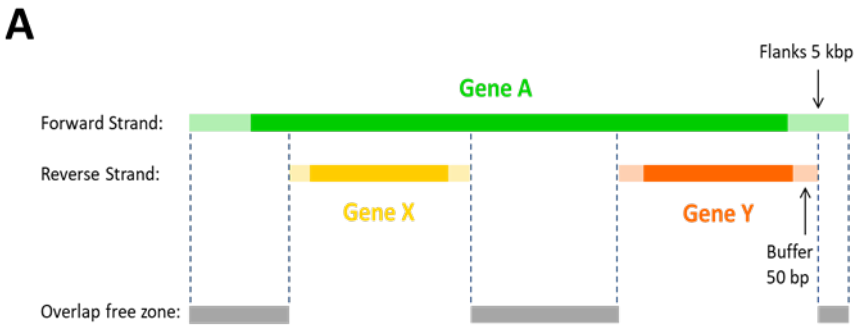

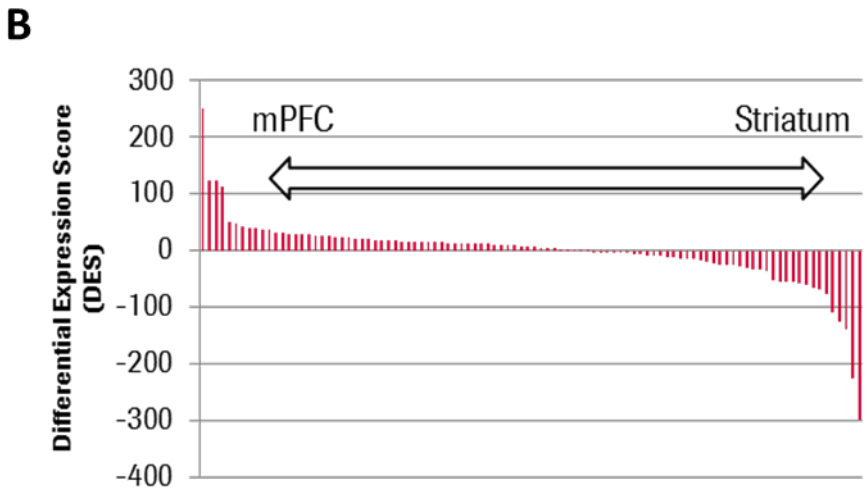

C

Genes with five highest DES (mPFC-enriched)

Gene	DES
Rpe65	251.86
Agtr2	124.13
Ap1s2	123.97
Gamt	112.23
Mkks	50.03

D

Genes with five lowest DES (Striatum-enriched)

Gene	DES
Prss12	-298.98
Mef2c	-226.17
Rpgrip1l	-138.29
Syn1	-126.72
Kras	-108.80

Figure 3. Identifying and Profiling Antisense Reads.

A. Schematic explaining the methodology we used to define antisense reads around ASD-related genes. Autism-related Gene A locus (dark green) and corresponding 5 kbp flanking region (light green) are aligned to reverse strand and reads in the corresponding region were identified as antisense reads. In the presence of a genomic element on the reverse

stand (in this example Gene X and Gene Y), gene locus (yellow and orange areas) and a 50 bp-buffer around these elements (light yellow and light orange) were removed from the antisense read count. Remaining overlap free zones (gray areas) were used in analyses. **B.** 100 ASD-related genes sorted according to their differential expression score. Higher score indicates mPFC-enriched, while lower score indicates striatum-enriched-expression. **C.** Top 5 genes with most mPFC-enriched antisense read counts. **D.** Top 5 genes with most striatum-enriched antisense read counts.

Significant Fraction of Sense and Antisense Reads Displayed Strong Negative Total Correlation

Similar to differential spatial expression, correlation of reads could also indicate a possible regulatory, functional mechanism for antisense reads. For example, *SYNGAP1*-antisense was demonstrated to have an enriched expression in prefrontal cortex (PFC) and superior temporal gyrus, and a significant negative correlation with *SYNGAP1* expression in PFC (63). Therefore, we investigated the strength of correlation between sense and antisense reads. We first compared the average expression levels of sense and antisense reads across brain development (P7, P14 and P56). We applied the Pearson coefficient correlation to reveal the relationship between sense and antisense read expression through development. Correlation analysis revealed that a fraction of sense and antisense reads had a positive or negative correlation (Fig. 4A). Around 5% of reads had a strong positive correlation (correlation coefficient $r > 0.90$, see Fig. 4B for top 5 genes with positive correlation), while 20% of reads had a strong negative correlation (correlation coefficient $r < -0.90$, see Fig. 4C for top 5 genes with negative correlation) (see additional files for complete list). Interestingly, *Ube3a*, a gene known to be negatively regulated by *Ube3a*-antisense transcript (173), showed a strong positive correlation between sense and antisense reads.

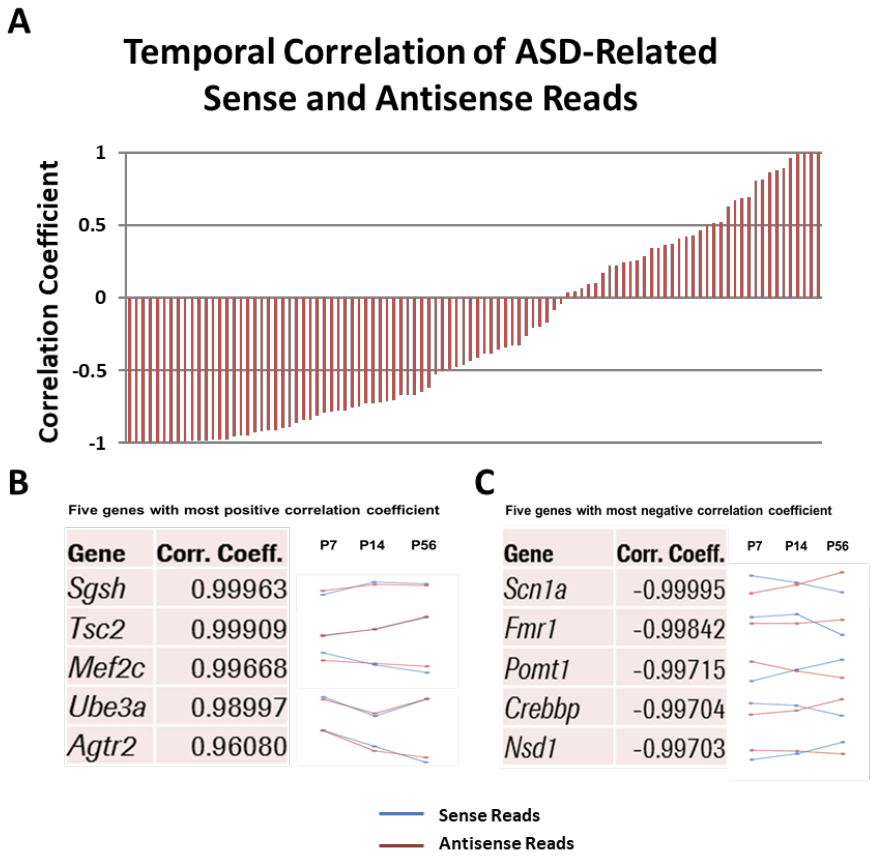

Figure 4. Correlation of Sense and Antisense Reads for 100 ASD-Related Genes

A. 100 genes were sorted (X-axis) based on the correlation coefficient between their sense and antisense reads. A correlation coefficient of 1 indicates a perfect positive correlation, while -1 indicates perfect negative correlation. **B.** Genes with highest correlation coefficient for their sense-antisense reads. **C.** Genes with lowest correlation coefficient for their sense-antisense reads.

A Novel *De Novo* Transcriptome Assembly Approach Identified Putative ASD-Related Natural Antisense Transcripts

A comprehensive antisense transcriptome is lacking for mouse genome with mPFC and striatum specific annotations. To fulfill this need, we used deep RNA sequencing to assemble a non-coding RNA transcriptome from mouse mPFC and striatum samples. We used a novel bioinformatics approach for verifying the resultant contigs after assembly by blasting them back to the mouse genome (Fig. 1). Our verification approach reduced ~100,000 contigs to ~70,000 that were assembled from the antisense strand of coding genes for the entire genome (see additional files for complete list in FASTA format). This is a significant number given that there are about 20,000 estimated protein coding genes identified in mouse.

Principal component analysis (PCA) of the assembled contigs revealed a clear clustering based on brain region (niche) and developmental stage (age) (Fig. 5A). This clearly demonstrates that assembled *de novo* contigs can successfully be used to distinguish samples based on their tissue origin and age. We next focused our analyses to ASD-related contigs that were differentially expressed across niche and age (Fig. 5B). We identified many contigs that were differentially expressed both in niche and age axes (see additional files for complete list).

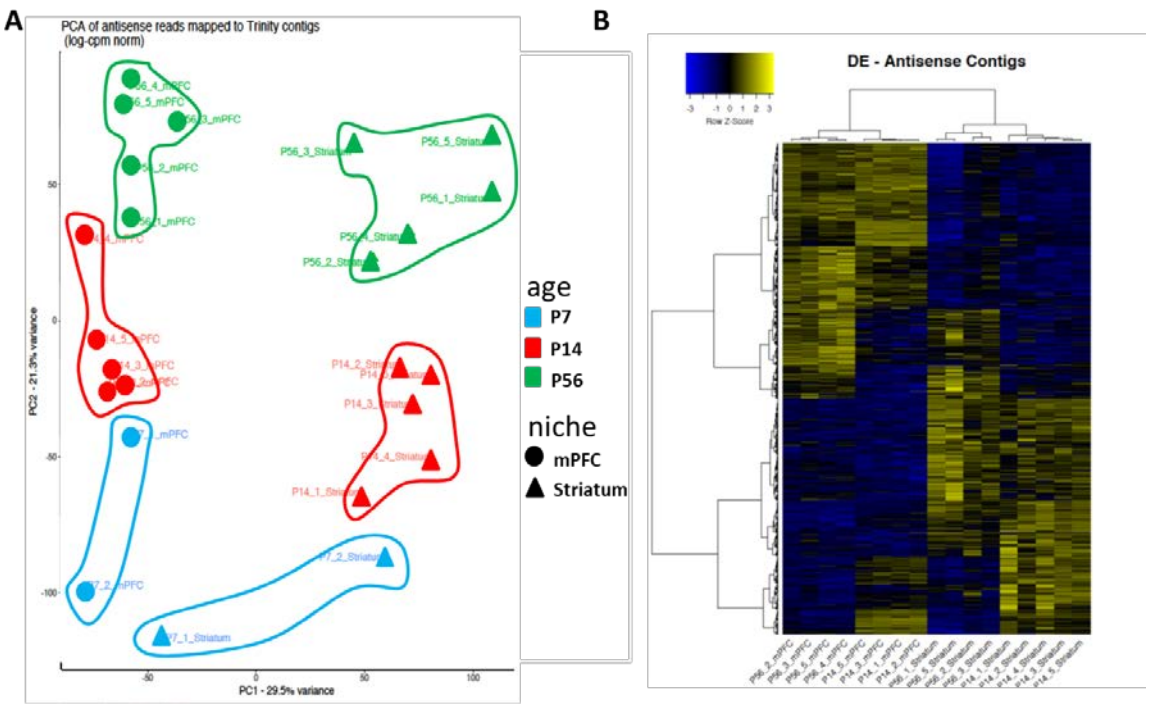

Figure 5. ***De Novo*** **Antisense Transcriptome of Mouse mPFC and Striatum**

A. Principal component analysis of assembled contigs revealed clustering of samples based upon both their tissue origin (X-axis) and developmental age (Y-axis). **B.** Differential expression analysis of ASD-related contigs showed significant brain region and age-specific expression (see additional file for complete list with statistical significance values).

A Subset of ASD-Related Contigs Showed >90% Complementarity to Human

It is important to reveal the homology between mouse and human antisense transcripts both for understanding how these transcripts were emerged through evolution and for targeting them in model organisms to study their functions. To define candidates for ASD-related transcripts in mice, we blasted our *de novo* antisense contigs against the human genome to determine highly conserved transcripts. Our analysis revealed a fraction of antisense contigs that had >90% coverage and >90 complementarity to their respective human gene locus (Table 2).

Table 2. ASD-related antisense contigs that are >90% complementary to human orthologues

Related Gene	Antisense ID
Mef2c	ENSMUSG00000005583_Mef2c_antisenseF_57
Mef2c	ENSMUSG00000005583_Mef2c_antisenseF_65*
Mef2c	ENSMUSG00000005583_Mef2c_antisenseF_165
Mef2c	ENSMUSG00000005583_Mef2c_antisenseF_172
Mef2c	ENSMUSG00000005583_Mef2c_antisenseF_183
Crebbp	ENSMUSG00000022521_Crebbp_antisenseR_1*
Crebbp	ENSMUSG00000022521_Crebbp_antisenseR_2
Nrxn1	ENSMUSG00000024109_Nrxn1_antisenseR_5
Nrxn1	ENSMUSG00000024109_Nrxn1_antisenseR_19
Rpgrip1l	ENSMUSG00000033282_Rpgrip1l_antisenseR_37*
Braf	ENSMUSG00000002413_Braf_antisenseR_7
Scn1a	ENSMUSG00000064329_Scn1a_antisenseR_6
Pten	ENSMUSG00000013663_Pten_antisenseF_5
Foxp1	ENSMUSG00000030067_Foxp1_antisenseR_28*

*Undergone expression validation by qPCR.

Expression Validation of *De Novo* Antisense Contigs as Putative ASD-Related Natural Antisense Transcripts

Next, we selected some of the highly conserved (Table 2) and non-conserved ASD-related antisense contigs for qPCR verification. We used a combination of criteria for selecting non-conserved contigs (ENSMUSG00000039419_Cntnap2_antisenseF_13, ENSMUSG00000027978_Prss12_antisenseF_10,

ENSMUSG00000067629_Syngap1_antisenseF_4,
ENSMUSG00000067629_Syngap1_antisenseF_9,
ENSMUSG00000051331_Cacna1c_antisenseR_15) such as predicted antisense expression in human (*Syngap1*, *Cacna1c*, *Cntnap2*) and suggestive evidence for a regulatory role in the mouse brain. For example, *Prss12* had strong mPFC-enriched sense (Fig 1B) and striatum-enriched antisense expression (Fig 3D) with a high opposite read score (Table 1).

We designed custom TaqMan probes for the selected transcripts (see additional files for list of selected transcripts and TaqMan probe sequences) and validated their presence by qPCR using total RNA isolated from mouse brain tissue (Fig. S2). We confirmed the size of the expected PCR-products by agarose gel electrophoresis (Fig. S2) except for one sample. Given that we could successfully confirm the presence of all selected *de novo* contigs by qPCR, we consider them as putative natural antisense transcripts but their functional significance awaits further testing

Discussion

Here, we investigated the differential expression of 100 ASD-related genes and their antisense partners in mouse using a highly deep RNA sequencing approach (120 million reads/sample). Our comprehensive study provides a deep understanding of how ASD-related antisense transcripts are differentially regulated in two ASD-associated brain tissues (mPFC and striatum) through brain development. To the best of our knowledge, our study is unique for dissecting NAT expression at such resolution and providing brain region specific and developmental information. Moreover, we assembled a *de novo* antisense transcriptome resulted in 70,000 contigs that were verified by blast analysis and identified a subset with high human complementarity. Our *de novo* antisense transcriptome can be used as a point of reference for selecting NAT candidates in CNS research.

Majority of publicly available RNA-Seq datasets are lacking strand-specific information that is essential for determining sense-antisense information (174) or they use poly(A)-enriched RNA libraries as starting material (175). Since not all lncRNAs have poly(A) sites (70), we used total RNA to capture all RNA species including non-poly(A) transcripts in our libraries and used strand-specific sequencing approach to extract sense-antisense information. Moreover, lncRNAs are expressed relatively low levels compared to protein coding mRNAs (67, 79, 176). In order to detect lncRNAs expressed at lower levels, we used a deep sequencing approach that had a resolution of 120 million reads/sample. Therefore, our study is more likely to provide a more complete list of antisense transcripts expressed in mouse brain.

100 genes we used in this study do not represent all ASD-related genes. For example, 1,503 human genes implicated in autism are listed by SFARI gene database as of January 15, 2019 (https://www.sfari.org/resource/sfari-gene/). However, our list provides a good one-to-one comparison with the study where expression of human NATs were examined for the same ASD-associated genomic regions in human (63). For example, *SYNGAP1*-antisense was shown to be differentially expressed in autistic brains compared to the brains of control subjects. No *Syngap1* antisense transcript has been reported so far in mice or rats; therefore, using animal models to study NAT-mediated gene regulation of *Syngap1* has not been possible. In our *de novo* antisense transcriptome, we could assemble several antisense transcripts that are related to *Syngap1* locus and validated the expression of ENSMUSG00000067629_Syngap1_antisenseF_4 and ENSMUSG00000067629_Syngap1_antisenseF_9 in mouse brain tissue by qPCR (Table 2). If regulatory functions of these transcripts could be demonstrated, they would serve as a novel modality to regulate *Syngap1* expression in mice similar to *Ube3a* (157), *Bdnf* (102), *Bace1* (177) among others.

Brain region-enriched expression can pinpoint a specific function for the investigated gene or transcript. For example, *Foxp1* is a good example for an autism-related gene demonstrated with a striatum-specific function (178). Foxp1 regulates excitability of medium spiny neurons in striatum and its reduction was correlated with ultrasonic vocalization deficits in mouse. In parallel to this finding, our analysis demonstrated that *Foxp1* was the most differentially expressed gene in striatum (Fig. 2B). Similarly, developmental regulation of genes can also indicate specific functions affecting brain development. A good example for an ASD-related gene that is known to be developmentally regulated is doublecortin (*Dcx*) (179, 180). Mutations in *Dcx* cause neuronal migration deficits and are associated with mental retardation (181). As expected, *Dcx* stood out as one of the most developmentally regulated genes in our analysis, its expression was downregulated from P7 to P56 (Fig. 2D). For example, *Prss12* is a particularly interesting gene that it showed strong mPFC-enriched sense (Fig 1B) and striatum-enriched antisense expression (Fig 3D) with a high opposite read score (Table 1). A greater interest could be drawn for the genes and antisense transcripts identified as developmentally or spatially regulated to reveal their function in ASD.

By restricting our search for antisense reads to ASD-related gene locus and its 5 kbp flanking region (Fig. 3A), we aimed to identify NATs that are known to have sequence complementarity with their protein-coding partners. We also removed genomic elements that were present on the reverse strand of ASD-related genes to eliminate any abundance contribution by protein-coding genes. We are not aware of any example where a protein-coding gene can act as an antisense transcript to regulate the expression of another protein-coding gene in the reverse strand. In case such regulation is present, we might have biased our search and excluded protein-coding genes with antisense function.

Expression correlation of sense and antisense partners might indicate a functional relationship. Several studies have tried to understand the link between sense-antisense transcript pairs by analyzing their correlation relationship (99). For example, a positive correlation was reported for sense-antisense partners that show tissue-specific expression profiles with overlapping promoter sequences (182). On the other hand, a negative correlation was identified for antisense transcripts that position in the introns or downstream of their protein-coding partners (183). In our study, we observed nearly a binary distribution for the temporal correlation of sense and antisense expression (Fig. 4A) with more genes showing negative correlation. For example, *Ube3a* is a known gene with antisense-mediated expression regulation (157) and it showed a strong positive correlation (Fig 4B). On the other hand, *Scn1a*, a gene known to have an antisense gene in mouse (184), showed a strong negative correlation (Fig 4C). Therefore, we cannot speculate with our dataset for any mechanism attributable to temporal correlation of sense and antisense partners.

Our *de novo* antisense transcriptome is a great resource with over 70,000 assembled contigs with mPFC and striatum specific annotations. The PCA of assembled transcripts resulted in a clear clustering of samples based on their brain region (niche) and development (age) (Fig. 5A). Our differential expression analysis also revealed many of these contigs were significantly tissue and age specific (Fig. 5B). Given that ncRNA expression can be exceptionally specific to cell types, neuroanatomical regions and subcellular compartments (81), our findings are also consistent with the idea that lncRNAs play functional role in CNS development and diseases (74).

With our novel bioinformatics approach using masking and blast verification of assembled transcripts (Fig. 1), we could significantly refine initially assembled ~100,000 contigs by ~30%. Therefore, we are confident that the majority of these contigs are actual antisense

transcripts present in the brain. Successful validation of all 9 selected contigs by qPCR in the mouse brain (Fig. S2) also goes in favor of the precision of our approach. Nevertheless, validation of these contigs as functional transcripts is necessary. For example, cell based, large-scale RNA interference-mediated loss of function assay (185) can be used to validate biological function of the assembled transcripts.

Conserved sequences of antisense transcripts between mice and humans could indicate a shared mechanism and facilitates experimental efforts to understand the functionality of antisense transcripts using animal models. By blasting our assembled novel *de novo* antisense transcripts against the human genome, we could identify highly complementary and covered sequences between two species for ASD-related genes (Table 2). *Mef2c* is particularly interesting as it has several contigs that are highly complement with the human locus, and many Mef2c contigs are differentially expressed (Fig. 5B). Multiple non-coding and antisense RNAs have been identified around human *MEF2C* gene (186); however, no antisense transcript has been reported for the mouse homolog. Hence, investigating antisense regulation of *Mef2c* in mouse would be noteworthy. Nevertheless, it is also important to note that sequence homology is not the only parameter that determines similar functions in different species (187). For instance, the brain-derived neurotrophic factor gene (*Bdnf*) in mouse and human are regulated by their respective *Bdnf*-antisense transcripts despite lack of conserved antisense sequences between two species (102). Therefore, a more inclusive approach should be considered when antisense transcripts are compared between two or more species.

Conclusions

The data presented here provide evidence that some ASD-related genes and their antisense transcripts are differentially expressed between mPFC and striatum through development. These differences should be taken into account to obtain a more complete view of the

interplay of sense-antisense partners that lead to the disease state. Moreover, we successfully assembled *de novo* antisense transcriptome with over 70,000 contigs for mouse brain with tissue specific annotations. Our antisense transcriptome can be used as a reference for determining NAT candidates for research activities in the CNS and its disorders. Our novel bioinformatics approach to verify and mask contigs provides a more refined list of transcripts and it can be applicable to other *de novo* transcriptome assembly studies. Identifying and understanding specific antisense transcripts regulating the expression of ASD-related genes would be important to develop novel RNA-based therapeutics (98) for ASD.

Abbreviations

ASD: Autism spectrum disorder **mPFC**: Medial prefrontal cortex **Str**: Striatum **RT-qPCR**: Quantitative reverse transcription real-time PCR **PCA:** Principal component analysis **NAT:** Natural antisense transcript **ncRNA:** non-coding RNA **kbp:** kilo base pair **RPKM:** Reads per kilobase transcript

Acknowledgments

We thank Keith Gunapala for editorial support and the Hall Lab for invaluable comments on the manuscript.

Author Contribution

Full support was provided by F. Hoffmann-La Roche Ltd. of Basel, Switzerland, where B.K., R.S., N.G., T.B., and B.J.H. were full time employees during the course of studies. B.K., G.F., R.S., T.B. and B.J.H. conceived and designed the experiments. B.K. performed all wet lab

experiments except for RNA-Seq which was done by N.G. B.K., G.F., and R.S. analyzed the data. B.K. and B.J.H. drafted and revised the manuscript.

Supplementary Figures

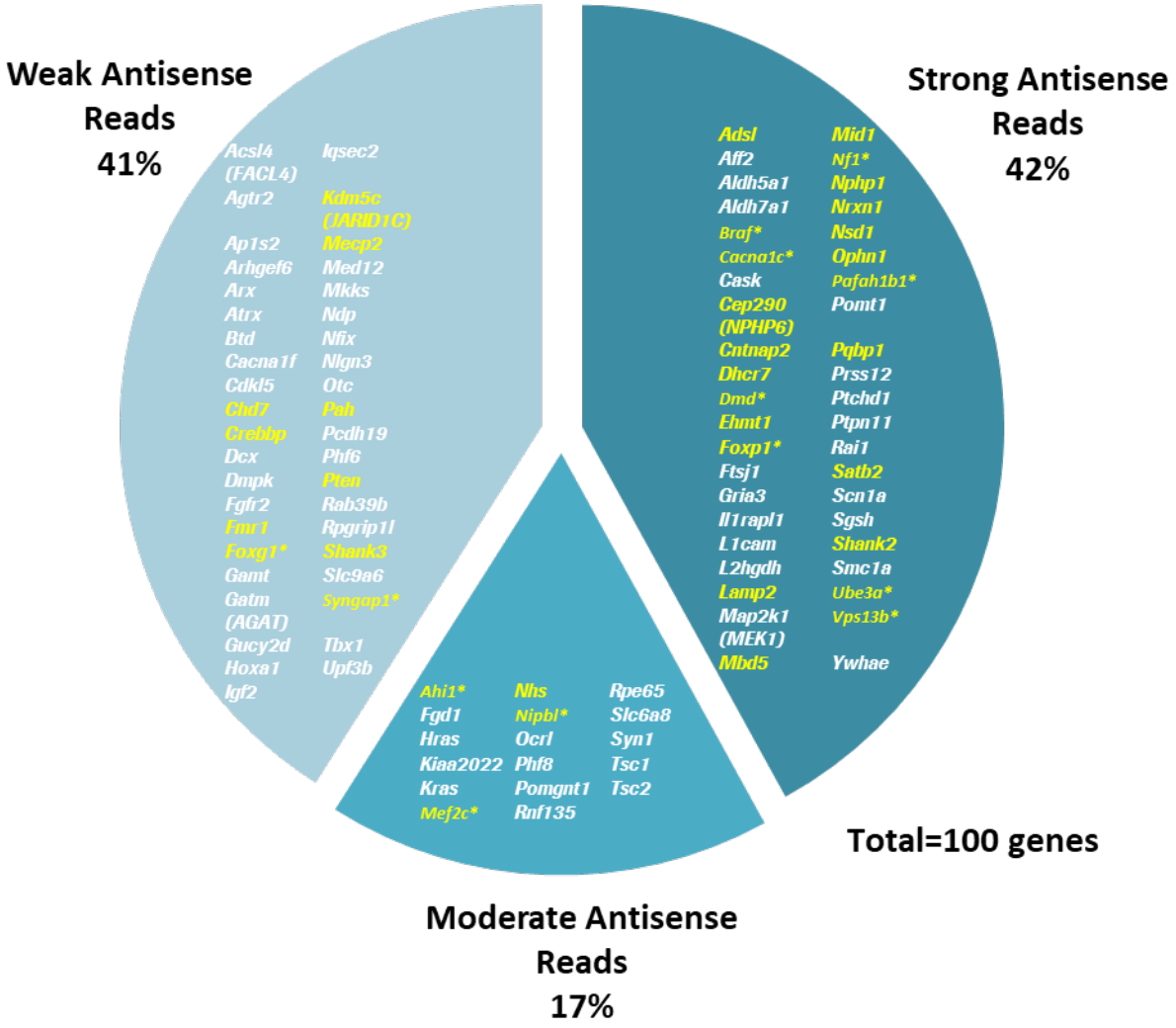

Figure S1. Qualitative classification of ASD-related genes based on the abundance of their antisense reads.

100 out of 103 autism-related genes with 1-1 murine orthologues (Ensembl Release 90) were qualitatively classified based on the abundance of their antisense reads into three categories: strong antisense reads (42%), moderate antisense reads (17%), weak antisense reads (41%). Yellow highlighted genes have NATs in humans: 23/37 genes (~62%) overlapped also for clear antisense reads in mice. Asterisk (*) indicates the presence of at

least one NAT in brains of Cynomolgus macaque (Aceview, NHPRTR Project). Common NATs in all three species: Braf, Cacna1c, Foxp1, Nf1, Pafah1b1, Ube3a, Vps13b.

No	Antisense ID	qPCR Verification
1	Mef2c_F_65	Yes
2	Crebbp_R_1	Yes
3	Rpgrip1l_R_37	Yes
4	Foxp1_R_28	Yes
5	Cntnap2_F_13	Yes
6	Prss12_F_10	Yes
7	Syngap1_F_4	Yes
8	Syngap1_F_9	Yes
9	Cacna1c_R_15	Yes
+	18S	Yes

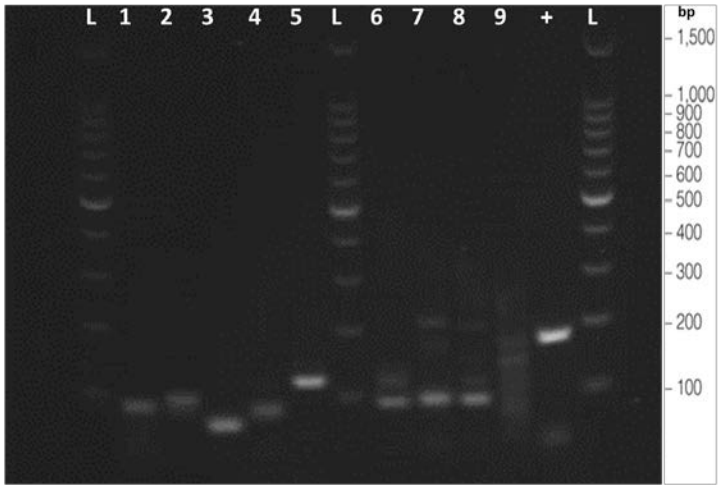

Figure S2. Verification of Selected *De Novo* Contigs as Natural Antisense Transcripts

Left panel: 9 antisense de novo contigs were verified using custom made TaqMan Probes in RT-qPCR. 18S transcript was used as a positive control. + is positive control. **Right panel:** Agarose gel electrophoresis of the RT-qPCR products. All RT-qPCR products of antisense transcripts, except for Cacna1c_R_15 (9), separated to expected fragment size. L is DNA ladder, bp is base pair.

Supplementary Materials

HBSS

- 25 ml 10x HBSS (Thermo Fisher Scientific, Catalog# 14185052)
- 625 µl 1 M Hepes (Thermo Fisher Scientific, pH 7.4) (Catalog# 15630056)
- 3 ml 2.5 M Glucose (Sigma, Catalog# G8769)
- 1.5 ml 1 M $MgCl_2$ (Sigma, Catalog# 63069)
- 250 µl 1 M $CaCl_2$ (Sigma, Catalog# 2115)

Under sterile hood, ingredients were mixed and added nuclease-free H_2O (Thermo Fisher Scientific, Catalog# 10977-035) to 250 ml and sterile filtered.

Chapter 2 - Diverse Modes of NMDA Receptor Antagonism Disrupt Working Memory by Affecting Different Behavioral Measures

Baran Koç[1, 2], Eoin C. O'Connor[2], Benjamin J. Hall[2]

1- Faculty of Science, University of Basel, 4056 Basel, Switzerland

2- Pharma Research and Early Development, Neuroscience Discovery, Roche Innovation Center Basel, 4070 Basel, Switzerland

Correspondence to Benjamin J. Hall (benjamin.hall@roche.com).

Abstract

NMDA receptors (NMDARs) are critical regulators of synaptic plasticity and therefore cognitive behavior. Dysfunction in NMDARs has been associated with cognitive impairment in various neurological diseases. NMDAR antagonism has been used to model cognitive dysfunction in animal studies; however, how these antagonists impair the working memory domain of cognition is not fully understood. In this study, we measured the effects of NMDAR antagonism on working memory in mice, using a translatable, touchscreen-based operant task (TUNL) and treating animals with non-subunit selective uncompetitive antagonists MK-801 or ketamine, as well as the GluN2B-subunit selective antagonist RO 25-6981. Treatment with MK-801 or RO 25-6981 impaired working memory performance while, ketamine, at a pro-motivational low dose, did not have any significant effect. By dissecting the TUNL task into quantifiable components, we found that MK-801 significantly increased choice latency –suggesting an impairment in decision execution. On the other hand, RO 25-6981 caused an impulsive, inattentive behavior evident as a reduction in all task latencies measured. By combining systemic NMDAR antagonism with genetic suppression of GluN2B or the NMDAR-associated gene *Syngap1* in medial prefrontal cortex

(mPFC), we observed that loss of GluN2B exacerbated the MK-801-induced working memory impairment while *Syngap1* knockdown animals showed reduced impairment. Our findings provide insight into how NMDARs and an associated cellular signaling molecule contribute to specific features of working memory in mPFC circuits.

Introduction

N-methyl-D-aspartate receptors (NMDARs) are ionotropic glutamate receptors that regulate excitatory synaptic transmission and plasticity (188). NMDARs are heterotetramers composed of two GluN1 subunits and two GluN2A or GluN2B subunits. Diversity in receptor composition regulated through GluN2A and GluN2B subunits has an impact on receptor properties and function (33). Due to their role in synaptic plasticity, NMDARs are strongly involved in cognitive functions (189). NMDAR hypofunction has been linked to cognitive dysfunction such as executive function deficits, attentional processing, working memory impairment (122). NMDAR antagonists are widely used to mimic cognitive dysfunction in animal models (129, 131).

The Trial-Unique Non-Matching to Location (TUNL) task is used to assess spatial working memory in rodents and is translatable to humans (112, 118). In TUNL, an automated operant chamber allows working memory assessment by requiring the animal to choose a nonmatching location after a variable delay following a sample phase. In this way, detailed assessment of working memory parameters is possible due to precise measurement of task parameters such as response latencies (113).

The effects of NMDR antagonism on spatial working memory in TUNL have been tested mainly in rats. Systemic injection of MK-801 impaired working memory performance while GluN2A-specific NVP-AAM077 or GluN2B-selective antagonists CP 101-606 and RO 25-6981 did not show any significant effect on test accuracy (129, 130). Lesion studies suggested

that mPFC (120) and (dorsal) hippocampus (112, 121) are brain regions involved in TUNL task.

The NMDAR-associated protein Syngap1 is a postsynaptic density associated protein present at excitatory synapses (51). As a downstream regulator of NMDAR signaling, Syngap1 plays a critical role in excitatory synapse function by negatively-regulating α-amino-3-hydroxy-5-methyl-4-isoxazolepropionic acid receptor (AMPAR) levels (56). Loss of function mutations in *SYNGAP1* have been implicated in intellectual disability and autism spectrum disorder (61, 190). Animal models of *Syngap1* dysfunction recapitulate similar behavioral and physiological deficits seen in patients (136-139, 141). Interestingly, *Syngap1* heterozygous mice showed working memory deficits in an automated eight-arm radial maze working memory task (136).

The medial prefrontal cortex (mPFC) is a major center for working memory and executive function (191). Recently, thalamic projections to the mPFC have been suggested to sustain attentional control and activity during working memory maintenance (192, 193). Furthermore, synaptic input to the mPFC from the medial dorsal thalamus (MDT) is regulated by strong contribution of GluN2B-containing NMDARs and activation of this circuit drives increased motivated behavior (194). We previously showed *in vitro* that Syngap1 is preferably located in the GluN2B-containing NMDAR pathway (50). Based on these findings, we hypothesized that GluN2B and Syngap1 could have a role for working memory regulation in the mPFC by regulating MDT → mPFC inputs.

Herein, we tested the effect of systemic NMDAR antagonism on working memory in TUNL. Both subtype-nonspecific and GluN2B-selective antagonism impaired working memory performance, although low-dose ketamine did not alter performance. By using comprehensive cognition-related behavioral measures, we elucidated how these antagonists impaired working memory performance. Furthermore, by using conditional

viral vectors, we investigated how NMDAR antagonism was affected when GluN2B was deleted in the mPFC or *Syngap1* was knocked down in the excitatory cell population of the mPFC. We demonstrated that MK-801-induced working memory impairment was exacerbated with GluN2BΔmPFC while significantly alleviated by *Syngap1* knockdown.

Methods

Molecular Biology

For *Syngap1* silencing studies, shRNA constructs and respective scrambled controls were designed and incorporated into p*Silencer*™ siRNA expression vector (Thermo Fisher Scientific, Waltham, MA, USA) (Supplementary Materials and Methods for siRNA target sequences and RT-qPCR protocol). Constructs were tested in mouse primary cortical culture for their knockdown efficacy by RT-qPCR. The most effective constructs were incorporated into a conditional shRNA expression vector - pSico, which was a gift from Tyler Jacks (Addgene plasmid # 11578; http://n2t.net/addgene:11578; RRID:Addgene_11578) (195). AAV production from these constructs was performed by the Viral Vector Facility (VVF) of the Neuroscience Center Zurich (NCZ) (Fig. S6A). SynGAP knockdown by our custom designed viruses was assessed in mouse primary cortical culture (Fig. S6B-C).

Subjects

Male, homozygous GluN2B^{flox} (B6129S background) and homozygous Emx1-Cre (C57/BL6) mice up to 1 year of age at the time of analysis were used for all studies. GluN2B^{flox} mice were used under a license from Vanderbilt University (5). Emx1-Cre knockin mice (196) were obtained from the Jackson Laboratory. Regular tap water and food were available *ad libitum* except during TUNL experiments. During TUNL testing, body weight was maintained at 85-90% of free feeding levels by mild food restriction. Mice were bred and

group housed when possible in a colony maintained on a 12-hour light/dark cycle. TUNL experiments were performed in the dark phase under red light. Experiments were conducted in adherence to the Swiss federal ordinance on animal protection and approved by Canton of Basel-Stadt Veterinary Authority.

Surgical Procedures

Surgical procedures were followed as previously explained in detail by our lab (194). Briefly, after anesthetic plane was confirmed, viruses were injected bilaterally into the mPFC (ML: ± 0.30 mm, AP: 1.94 mm, DV: -2.50 mm) defined by Paxinos and Watson (197) and the Allen Mouse Brain Atlas (198), and were confirmed empirically. Total volume per injection was 200 nl per hemisphere. For post-op recovery and viral expression, animals were kept in their home cage at least for 2 weeks before experimentation.

For GluN2B knockdown in the mPFC, homozygous GluN2B^{flox} animals were injected with either AAV2-CaMKII-GFP or AAV2-CaMKII-GFP-Cre vectors from Vector Biolabs. Characterization of the AAV2-CaMKII-GFP-Cre for its knockdown efficiency was previously performed by our laboratory (194). For *Syngap1* knockdown in forebrain excitatory neurons, *Emx1*-Cre animals were injected with either AAV8/2-mU6-loxTATA-hCMV-EGFP-loxTATA-shRNA(SynGAP_1477-scrambled)-hGHp(A)-hCMV-mCherry-hGHp(A) (Scrambled-siRNA) or AAV8/2-mU6-loxTATA-hCMV-EGFP-loxTATA-shRNA(SynGAP_1477)-hGHp(A)-hCMV-mCherry-hGHp(A) (SynGAP-siRNA) (Fig. S6).

TUNL

The TUNL protocol was modified from a previous study (121). Animals were adjusted to reversed light cycle at least for two weeks before training. In the last week of an adjustment period food restriction was initiated, and in the last two days animals were familiarized to TUNL boxes for 45 minutes/day by introducing sucrose pellets in the food magazine.

Animals were trained to associate pellet reward with a nose poke to a lit window in the Sample Training with no punishment to background touch (non-target window). Animals that could collect 30 pellets in 1 hour were proceeded to Initiation Training.

In Initiation Training, animals were punished by house light illumination and a 5-sec time-out in the case of a background touch. Incorrect trials were repeated until animal made a correct response. Total run time was 1 hour or collection of 40 pellets. Animals that could reach the criteria of minimum 20 total trials, >70% correct on average of 2 consecutive trials (max of 20% variation) started with TUNL training.

In TUNL training, spatially-separated non-centric windows were used. Animals started a trial with a nose poke to the food magazine to light a sample window. Following a nose poke to the sample window, the light is turned off and the food magazine would illuminate after a 2 s delay. Animals initiated the choice phase by nose poking the food magazine leading to illumination of both the sample and a novel choice (non-matching) window. In order to collect the food reward, animals had to nose poke the choice window which led to immediate delivery of a sucrose pellet reward in the food magazine and initiation of a 15 s inter-trial interval. A touch to sample window or non-lit window was punished by house illumination and 5 s timeout. The trial was repeated until the animal made a correct choice. Total run time was 40 correct trials or 1 hour, whichever was reached first. Animals were first trained in the maximal window spatial separation mode - level S3 - with was a 3 window-gap between sample and choice windows. Once animals reached the criteria of minimum 20 total trials, >70% correct on average of 2 consecutive trials (max of 20% variation) they were proceeded to S2 phase. S2 phase was identical to S3 except that there was only a 2 window-gap between the sample and choice windows. Once animals reached criteria for S2 phase they were entered into the probe phase.

In the TUNL probe, working memory was tested in the S2 phase by varying the delay between sample selection and choice initiation. Animals were given random delays of 2 s, 4 s or 6 s evenly distributed over 48 total trials. Total run time was completion of 48 trials or 1 hour. There were no correction trials in this phase. Nose pokes to non-choice window initiated a house light illumination followed by a 5 s timeout.

Drug Treatments

Within-subjects study design was used for drug applications and each animal received all doses in randomized order. There was at least 2-day baseline training between treatments. Vehicle was 0.3% Tween-80 in physiological saline for all experiments. MK-801 (Sigma, M107) was delivered subcutaneously, RO 25-6981 (Sigma, SML0495) and ketamine (Sigma, K1884) were delivered intraperitoneally 30 min before task initiation.

Data Analysis and Statistics

Data was analyzed by paired t test, repeated measures one-way ANOVA with the Geisser-Greenhouse correction or repeated measures two-way ANOVA, unless otherwise specified; and *post hoc* tests were used for detailed statistical analysis, as appropriate. All data is expressed as mean and standard error of the mean (SEM). Statistical tests were carried out with Prism 7 (GraphPad Software, San Diego, CA, USA). A *P*-value of <0.05 is considered significant and all data values are non-significant unless specified.

Results

Working memory performance worsened after subtype-unspecific or GluN2B-selective antagonism

To validate our mouse TUNL working memory assay, we trained two groups of mice from B6129S and C57BL/6 backgrounds. The majority of animals (>85%) from both backgrounds successfully completed training (15 out of 16 B6129S mice, and 14 out of 16

C57BL/6 mice). Both groups showed delay-dependent performance worsening as predicted (Fig. S1) although C57BL/6 mice were more susceptible to delay-dependent performance worsening (Fig. S1B).

To test the effects of NMDAR antagonism on working memory, we injected animals with the uncompetitive and non-selective NMDAR antagonist MK-801 (0.1 mg/kg), the GluN2B-selective antagonist RO 25-6981 (1.25 mg/kg, 5 mg/kg, 20 mg/kg) or a low-dose of the non-selective antagonist ketamine (3 mg/kg) using a within-subjects design, that is: each animal received all three treatments as well as vehicle control (Fig. 1A). MK-801 and RO 25-6981 treatment caused a significant worsening of test performance ($n = 8$, $P = 0.0012$ for MK-801; $n = 8$, $F_{(2.722, 19.05)} = 15.26$, $P < 0.0001$ for RO 25-6981) but the low-dose ketamine treatment was comparable to the control condition ($n = 8$, $P = 0.3050$) (Fig. 1B-D). RO 25-6981 treatment led to a severe hyperactive behavior, most obvious in animals treated with the highest dose (Supplementary Video 1 and 2). We tested animals with lower doses of RO 25-6981 (0.08 mg/kg and 0.31 mg/kg) to remove the confound of hyperactivity by RO 25-6981 treatment. Neither of the two lower doses showed a significant change in performance or latencies (Fig. S2) despite an observation of reduced hyperactivity, suggesting RO 25-6981 at lower doses has no effect on working memory performance.

Fig. 1

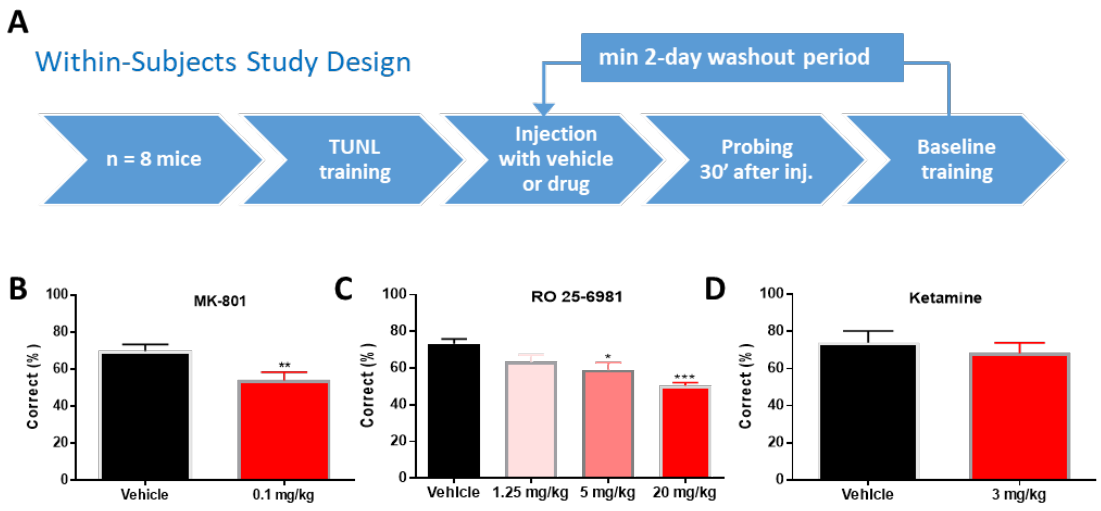

Figure 1. *Treatment with MK-801 or RO 25-6981 but not ketamine, impaired spatial working memory.* **A.** Schematic diagram detailing the within-subject experimental design. **B.** MK-801 (0.1 mg/kg) induced an impairment in working memory performance. **C.** Working memory performance decreased in a dose-dependent manner in response to RO 25-6981 (1.25-20 mg/kg) treatment. **D.** Low dose ketamine (3 mg/kg) did not cause any performance worsening of the working memory. Values show group mean ± SEM; $*P < 0.05$, $**P < 0.01$, $***P < 0.001$.

MK-801 and RO 25-6981 caused impairment in TUNL through different behavioral mechanisms

In order to elucidate how animals were impaired in TUNL due to NMDAR-antagonism, we dissected the TUNL task into its latency components (Fig. 2A). Both MK-801 and RO 25-6981 treatment showed decreased sample initiation latency (n = 8, $P = 0.0211$ for MK-801; n = 8, $F_{(1.688, 11.82)} = 14.53$, $P = 0.0009$ for RO 25-6981) (Fig. 2B-C). On the other hand, when we analyzed the choice latencies, interestingly we observed an opposite trend between MK-801 and RO 25-6981 conditions (Fig. 2D-E). Despite a general tendency of increased

engagement in the task for MK-801 treatment, choice latency in this condition was significantly increased (n = 8, $P = 0.0137$) suggesting an impairment in executive function or memory retrieval. In the RO 25-6981 condition, choice latency decreased in a dose dependent manner (n = 8, $F_{(1.975, 13.82)} = 2.875$, $P = 0.0909$ for drug, $F_{(7,21)} = 2.512$, $P = 0.0482$ for subjects, $P_{adj} = 0.0369$ for 20 mg/kg). RO 25-6981-treatment had a highly increased engaged behavior in the task (see within-subject comparison in Supplemental Video 1 after vehicle treatment, and in Supplemental Video 2 after 20 mg/kg RO 25-6981-treatment). However, this engaged state did not result in an attentive behavior, rather an impulsive behavior suggesting a possible explanation for reduced working memory performance.

We analyzed other parameters after NMDAR antagonism such as delay-dependent performance, the number of completed trials and task-related delays described in Fig. 2A. Delay-dependent performance impairment was less prominent both for MK-801 (Fig. S3A) and RO 25-6981 (Fig S4A) conditions likely due to the fact that animals started off with a lower baseline performance mainly for higher doses. The total number of completed trials increased in MK801 and RO 25-6981 treatment conditions (Fig. S3B & S4B) consistent with increased engagement in the task. However, this value was not significantly different presumably due to a ceiling effect imposed by limiting the maximum number of trials to 48. For other latency measurements (sample latency, choice initiation latency, and collection latency), MK-801-treatment did not show any significant difference although there was a trend for a decrease in latencies for the treatment condition (Fig. S3C-E). RO 25-6981 treatment also showed a trend for a decrease in latencies after treatment and in a dose dependent manner, and the decrease in sample and collection latencies were significant for higher doses but not for choice initiation latency (Fig. S4C-E).

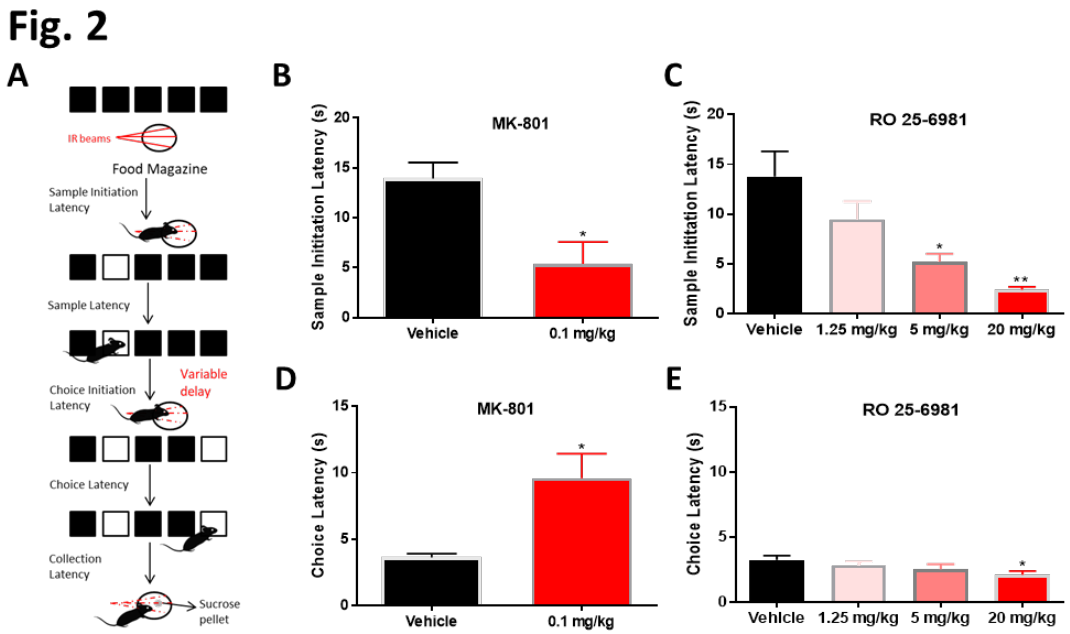

Figure 2. *Sample initiation latency increased after either MK-801 or RO 25-6981 treatment while choice latency was significantly altered in opposing directions.* **A.** Schematic representation of latencies measured. **B.** MK-801 treatment decreased sample initiation latency. **C.** RO 25-6981 treatment induced a dose-dependent decrease in sample initiation latency. All doses are compared to the vehicle. **D.** MK-801 treatment increased choice latency. **E.** Choice latency was decreased after RO 25-6981 treatment in a dose-dependent manner. All doses are compared to the vehicle. Values show group mean ± SEM; $*P < 0.05$, $**P < 0.01$.

mPFC-specific knockdown of GluN2B did not affect spatial working memory performance

Next, we wanted to test circuit specific role of GluN2B in mPFC for spatial working memory. We trained homozygous GluN2B^{flox} animals in TUNL and probed them to assess their spatial working memory (pre-injection). We then injected these animals either with AAV2-CaMKII-GFP (Control) or AAV2-CaMKII-GFP-Cre (GluN2BΔmPFC), to assess their behavior after removal of GluN2B from pyramidal neurons in mPFC (post-injection).

Both control and GluN2BΔmPFC animals showed improved performance after viral injection ($F_{(1,9)} = 6.431$, $P = 0.0319$) presumably due to the extended training time (Fig. 3A). Surprisingly, we did not observe any significant difference in performance following viral injection between control and GluN2BΔmPFC animals (Figure 3A, post-injection) ($F_{(1,9)} = 2.849 \times 10^{-5}$, $P = 0.9959$). Similarly, sample and choice latencies between control and GluN2BΔmPFC groups were comparable (Fig. 3B-C) ($F_{(1,9)} = 0.4568$, $P = 0.5161$ for sample initiation latency; $F_{(1,9)} = 1.445$, $P = 0.2600$ for choice latency) as well as performance at different delays, number of completed trials and other latency measurements (Fig. S5).

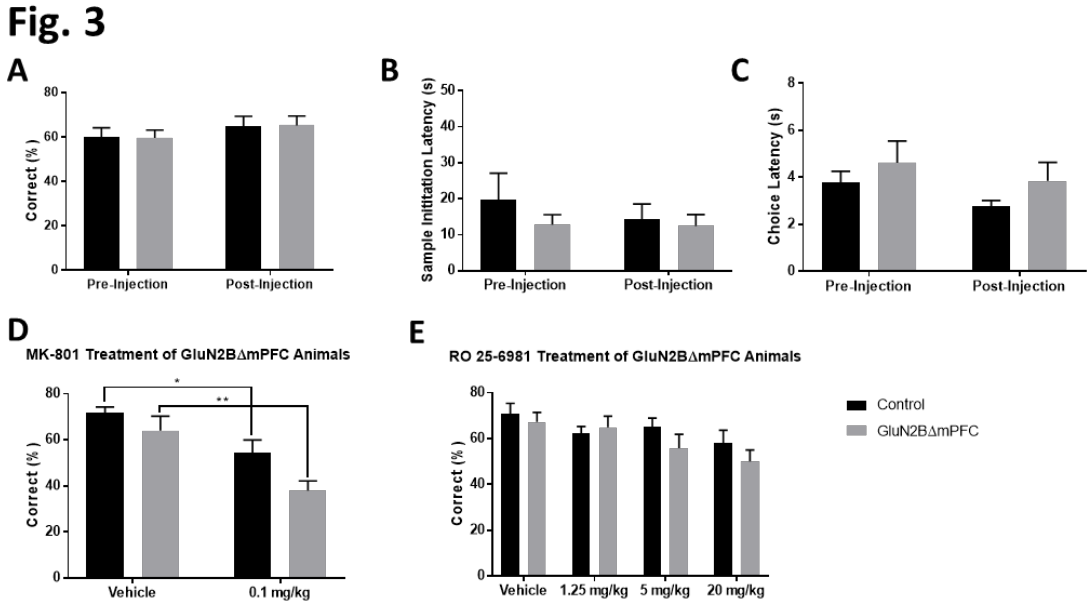

Figure 3. *GluN2BΔmPFC animals did not show any change in working memory measurements; however, they were more susceptible to MK-801-induced impairment.* **A.** Following GluN2B reduction in mPFC (post-injection), working memory performance was comparable to the control group. Both control and GluN2BΔmPFC animals showed improved performance after viral injection. **B.** Sample initiation latency analysis did not show any difference between control and GluN2BΔmPFC group after injection. **C.** Choice latency analysis did not show any difference between control and GluN2BΔmPFC group

after viral injection. **D.** MK-801-induced impairment in working memory was enhanced in GluN2BΔmPFC animals after viral injection. **E.** RO 25-6981-treatment did not yield any differences between control and GluN2BΔmPFC groups following viral injection. Values show group mean ± SEM; $*P < 0.05$, $*P < 0.01$.

GluN2BΔmPFC animals were more susceptible to MK-801-induced impairment but not to RO 25-6981

Although we did not observe a significant effect of GluN2B reduction in mPFC on working memory performance, we wanted to test whether GluN2BΔmPFC animals had any susceptibility or resistance to full or GluN2B-selective NMDAR antagonism. Interestingly, MK-801 treatment significantly exacerbated impairment due to non-selective NMDAR antagonism in GluN2BΔmPFC animals (Figure 3D) ($F_{(1,9)} = 38.12$, $P = 0.0002$ for drug effect, $F_{(1,9)} = 4.381$, $P = 0.0659$ for viral injection, $P_{adj} = 0.4690$ for vehicle, $P_{adj} = 0.0488$ for 0.1 mg/kg). GluN2B-selective antagonism by RO 25-6981 did not cause any significant change in working memory performance between control and GluN2BΔmPFC animals (Figure 3E) ($F_{(3,27)} = 4.998$, $P = 0.0069$ for drug effect, $F_{(1,9)} = 1.09$, $P = 0.3236$ for viral injection, $P_{adj} = 0.9692$ for vehicle, $P_{adj} = 0.9940$ for 1.25 mg/kg, $P_{adj} = 0.5102$ for 5 mg/kg, $P_{adj} = 0.6609$ for 20 mg/kg).

Syngap1 knockdown in mPFC did not affect working memory performance but led to reduced MK-801-induced impairment

We next tested the circuit specific effect of NMDAR-associated, schizophrenia risk gene *Syngap1* in mPFC. In order to achieve cell type-specific knockdown of *Syngap1*, we

designed, generated and characterized conditional shRNA-encoding viral vectors that express siRNA in the presence of Cre recombinase (Fig S6).

We first trained *Emx1*-Cre animals in TUNL and probed them for their spatial working memory (pre-injection). We then injected these animals with either scrambled-siRNA (control) or SynGAP-siRNA (SynGAP) viral vectors, and probed for their spatial working memory after recovery and baseline training (post-injection).

Both control and SynGAP animals had comparable levels of working memory performance after viral injection ($F_{(1,8)} = 0.2038$, $P = 0.2038$) (Fig. 4A). We did not observe any significant difference in performance following viral injection between control and SynGAP animals (Figure 4A) ($F_{(1,8)} = 0.3965$, $P = 0.5465$). Similarly, sample and choice latencies between control and SynGAP groups were comparable (Fig. 4B-C) ($F_{(1,8)} = 0.3229$, $P = 0.5855$ for sample initiation latency; $F_{(1,8)} = 0.3578$, $P = 0.5664$ for choice latency) as well as the performance at different delays, number of completed trials and other latency measurements (Fig. S7).

Similar to the GluN2BΔmPFC animals, we wanted to test whether *Syngap1*-knockdown in mPFC had any susceptibility or resistance to full or GluN2B-selective NMDAR antagonism. Interestingly, MK-801 treatment impairment was significantly reduced in SynGAP animals (Figure 4D) ($F_{(1,8)} = 12.69$, $P = 0.0074$ for drug effect, $F_{(1,8)} = 1.851$, $P = 0.2107$ for viral injection, $P_{adj} = 0.0284$ for Scrambled-siRNA, $P_{adj} = 0.2026$ for SynGAP-siRNA). GluN2B-selective antagonism by RO 25-6981 did not cause any significant change in working memory performance between control and SynGAP animals (Figure 4E) ($F_{(3,24)} = 5.606$, $P = 0.0046$ for drug effect, $F_{(1,8)} = 0.02551$, $P = 0.8771$ for viral injection, $P_{adj} = 0.9945$ for vehicle, $P_{adj} = 0.9326$ for 1.25 mg/kg, $P_{adj} = 0.9251$ for 5 mg/kg, $P_{adj} = 0.8915$ for 20 mg/kg).

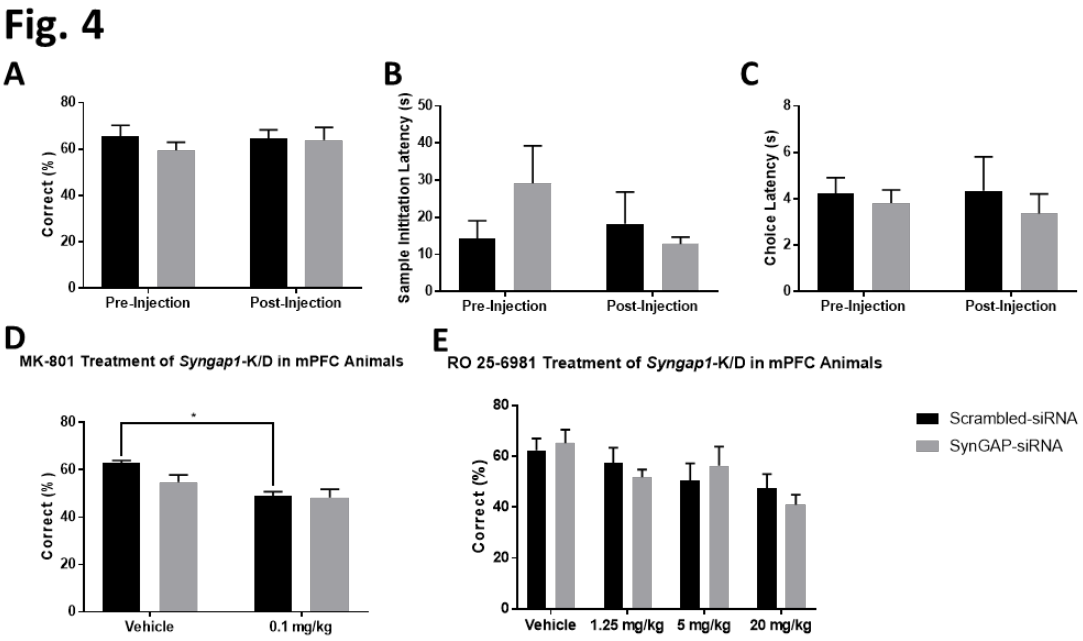

Figure 4. *Syngap1-knockdown animals did not show any change in working memory measurements; however, MK-801-induced impairment was reduced in SynGAP animals.* **A.** Following *Syngap1* knockdown in mPFC (post-injection), working memory performance was comparable with the control group. **B.** Sample initiation latency analysis did not show any difference between the control and SynGAP group after injection. **C.** Choice latency analysis did not show any difference between the control and SynGAP group after viral injection. **D.** MK-801-induced impairment in working memory was reduced in SynGAP animals after viral injection. **E.** RO 25-6981-treatment did not yield any differences between control and SynGAP groups following viral injection. Values show group mean ± SEM; $*P < 0.05$.

Discussion

In this study, we successfully developed the TUNL assay in mouse for pharmacological testing. We investigated NMDAR-antagonism on working memory performance in TUNL. Our results show that systemic MK-801 treatment impaired working memory performance with increased choice latency, suggesting an impairment in memory retention or decision

execution. NMDAR antagonist ketamine at a low, pro-motivational dose did not cause any significant effect on working memory performance. GluN2B-selective antagonism by RO 25-6981 impaired working memory performance in a dose-dependent manner. Despite reduced latencies (including choice latency) and increased task engagement after RO 25-6981 treatment, animals still failed to accomplish the task successfully presumably due to their increased impulsive and inattentive behavior. Furthermore, we investigated effects of mPFC-specific circuit manipulation on working memory by selectively deleting GluN2B or knocking down NMDAR-associated gene *Syngap1*. Interestingly, GluN2BΔmPFC exacerbated MK-801-induced impairment while *Syngap1*-knockdown blunted this effect.

Traditional working memory tasks such as T-maze, radial arm maze, delayed non-matching to sample, operant delayed-non-matching-to-position (DNMTP) generally provide overall performance as a readout for working memory assessment (117, 199). The main advantages of TUNL compared to these methods are that it allows experimenters to dissect the task into several quantifiable components mainly in the form of latency measures and provide multiple locations for choice phase to reduce body orientation bias as observed in DNMTP (118). In this study, we took advantage of latency measures to understand how different forms of NMDR antagonism affected working memory specifically. Despite common phenotype of reduced working memory performance after both MK-801 and RO 25-6981 treatment (Fig. 1 B-C), detailed analysis revealed that these antagonists actually affected different cognition-related functions to impair working memory –namely decision execution for MK-801 measured by increased choice latency (Fig. 2B), and impulsivity/attentional deficit for RO 25-6981 measured by decreased overall latencies (Fig. 2 C&E, Fig. S4 C-E) without working memory improvement. Furthermore, opposing choice latency measure observed between subtype-nonspecific and GluN2B-selective antagonism (Fig. 2D vs Fig. 2E) suggests that different NMDAR subunits might contribute to

working memory regulation by affecting diverse cognition-related pathways (122). Therefore, ability to distinguish cognitive features is particularly important to understand distinct biological basis of cognitive deficiencies present in schizophrenia, or neurodevelopmental disorders in general, and to define biological mechanisms.

A single, low dose of ketamine has a rapid antidepressant effect in treatment-resistant patients (200) and improves attentional processing in healthy controls by reducing the response time to target stimuli in visual oddball task for assessing attentional processing (201). In mice, low dose ketamine has a pro-motivational effect in the forced swim test and tail suspension test –both of which assess behavioral despair (135). Based on these findings, we hypothesized that a low dose ketamine treatment in mice could have a positive effect on working memory performance by improving motivation and task engagement. However, a low dose ketamine treatment (3 mg/kg) failed to cause a significant effect on working memory performance in TUNL (Figure 1D). We interpret this finding as ketamine's presumed pro-motivational effect was not sufficient to improve working memory performance especially in the absence of any cognitive dysfunction. This finding is also consistent with the fact that GluN2BΔmPFC alone did not result in any change in working memory performance (Figure 3A) as we previously demonstrated that *in vivo* deletion of GluN2B in mPFC mimics and occludes ketamine's positive actions on depression-like behavior (135).

The absence of any effect of genetic manipulations on working memory by GluN2BΔmPFC (Fig 3A-C) or *Syngap1* knockdown (Fig. 4 A-C) can be possibly explained by the fact that these manipulations alone might not be sufficient to induce any visible phenotype. Given that these animals did not possess any known susceptibility to cognitive dysfunction, their subtle effect might not be reflected in our study. Alternatively, our study might be underpowered to significantly reveal any subtle behavioral change caused by mPFC-specific

manipulations due to inadequate number of animals. Also the number or type of cells transfected by the virus might have contributed to the variation of the effect size. Increased baseline performance levels after viral injections (Fig. 3A), possibly due to prolonged training of animals, might also lead to a ceiling affect that prevents the detection of any improvement caused by viral manipulations. A more thorough investigation is necessary to rule out these experimental caveats. TUNL training time can be shortened by specific modifications or genetic knockdown approach can be used to study cognitive effects of GluN2B or Syngap1 reduction. For example, a recent study reported impaired cognitive flexibility following genetic GluN2B deletion in CaMKII-positive cell population (134). This study convincingly demonstrated that GluN2B deletion disrupted the coordination between orbitofrontal cortex and dorsal striatum by altering the neuronal firing rates that are necessary for optimal behavioral flexibility. It would be interesting to see whether GluN2B's role of mediating neuronal timing is applicable to other cognitive function, for example MDT → mPFC afferents in genetic GluN2B^{null} animals for sustaining activity during working memory maintenance.

Interestingly, in the case of cognitive dysfunction induced by MK-801, GluN2BΔmPFC resulted in an additional detrimental effect on working memory performance (Fig 3D) possibly enhancing pathway(s) that led to impulsive, inattentive behavior as induced by systemic GluN2B-selective RO 25-6981 treatment (Fig. 1C). On the other hand, cognitive dysfunction induced by MK-801 was blunted by mPFC-specific knockdown of *Syngap1* (Fig. 4D). This finding could be explained by a few possible mechanisms: first is that Syngap1 acts downstream of a subgroup of GluN2B-containing NMDARs that contribute to working memory regulation, second is that Syngap1 is preferably located downstream of NMDARs with other subunit composition such as GluN2A-containing, and last is that CaMKII (for GluN2B knockout) and Emx1 (for Syngap1 knockdown) promoters might be targeting

different cell populations. The last explanation is highly unlikely as Emx1 is known to be expressed in excitatory neurons (196), which also express CaMKII. Regarding the first two possibilities, the findings that Syngap1 preferably associates with GluN2B over GluN2A (57) and the absence of rescue effect of *Syngap1* knockdown in systemic GluN2B-selective antagonism (Fig. 4E) suggest that second explanation is less likely. In this case, that would be interesting to further investigate the heterogeneity of GluN2B-containing NMDARs and their distinctive roles in cognition.

A possible role for Syngap1 in the mPFC is that it might be located downstream of MDT to mPFC afferents that regulate working memory sustainment (192, 193). A mechanism we hypothesize for this role is that Syngap1$^+$ GluN2Bs are specifically receiving input from MDT that sustains attention, and knocking down the negative regulator *Syngap1* in this pathway disinhibits MDT to mPFC activity and contributes to enhanced working memory. A possible way to test this hypothesis would be injecting anterograde Cre-expressing viral vector in the MDT and co-injecting Cre-dependent Syngap1-siRNA virus in the mPFC. Another mechanistic explanation we can speculate is that Syngap1$^+$ synapses might be specifically receiving input from the ventral hippocampus (vHPC) that provides spatial encoding in working memory (202). In this scenario, *Syngap1* knockdown would facilitate the afferents coming from vHPC, thereby enhancing the spatial memory that is necessary for the TUNL task. Syngap1 and GluN2B synapses were also shown to be not always overlapping *in vivo* (38), so this mechanism could also explain the opposing phenotypes we observed between genetic GluN2B and Syngap1 reduction after MK-801 administration (Fig. 3D and Fig. 4D). Identifying downstream pathways of Syngap1$^+$ NMDARs in the mPFC would be also important for a thorough understanding of circuitry and brain regions involved in working memory regulation.

Altogether, our data provides an understanding of how different NMDAR subunits can affect working memory performance through distinct cognitive functionalities by applying a dissecting approach for working memory. We suggest a potential circuit mechanism that involves heterogeneous NMDAR subgroups with diverse molecular makeup for regulating different features of cognitive function. Our approach can be used to study biological mechanisms and distinct modalities of cognition and to develop and test therapeutics for neurodevelopmental diseases.

Acknowledgments

We acknowledge the Viral Vector Facility (VVF) of the Neuroscience Center Zurich (ZNZ) for generating AAV vectors for Syngap1 knockdown studies. The “G1uN2B foxed” mouse was generated by the Gene-Targeted Mouse Core of the INIA-stress consortium. This Integrative Neuroscience Initiative on Alcoholism examines the link between stress and alcohol. The consortium is supported by the National Institute on Alcohol Abuse and Alcoholism. The Gene-Targeted Mouse Core is supported by NIH grant UOl AA013514 (to Eric Delpire). We thank Roger Wyler and Marie Haman for their excellent technical support in TUNL experiments, Marie-Therese Miss, Vanessa de Barros and Charlotte Czernecki for animal colony maintenance, Keith Gunapala for editorial support, and Dr. Madhurima Benekareddy and the Hall Lab for invaluable comments on the manuscript.

Author Information and Disclosure

Full support was provided by F. Hoffmann-La Roche Ltd. of Basel, Switzerland, where B.K., E.C.O. and B.J.H. were full time employees during the course of studies. B.K., E.C.O. and B.J.H. conceived, designed and interpreted all experiments and revised the manuscript. B.K. acquired, analyzed all data and drafted the manuscript.

Supplementary Figures

Fig. S1

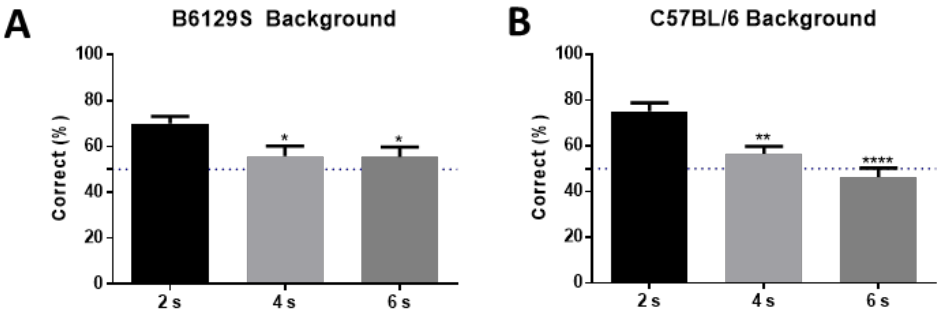

Figure S1. *Delay-dependent worsening of working memory performance in mice with different backgrounds* **A.** B6129S mice had a delay-dependent working memory worsening when introduced variable delays (n = 15, $F_{(1.968, 27.56)} = 4.968$, $P = 0.0147$, $P_{adj} = 0.0400$ for 4 s, $P_{adj} = 0.0295$ for 6 s, compared to mean of 2 s). **B.** C57BL/6 mice had a delay-dependent working memory worsening when introduced variable delays (n = 14, $F_{(1.89, 24.56)} = 21.31$, $P < 0.0001$, $P_{adj} = 0.0023$ for 4 s, $P_{adj} < 0.0001$ for 6 s, compared to mean of 2 s). Values show group mean ± SEM; *$P < 0.05$, **$P < 0.01$, ****$P < 0.0001$.

Fig. S2

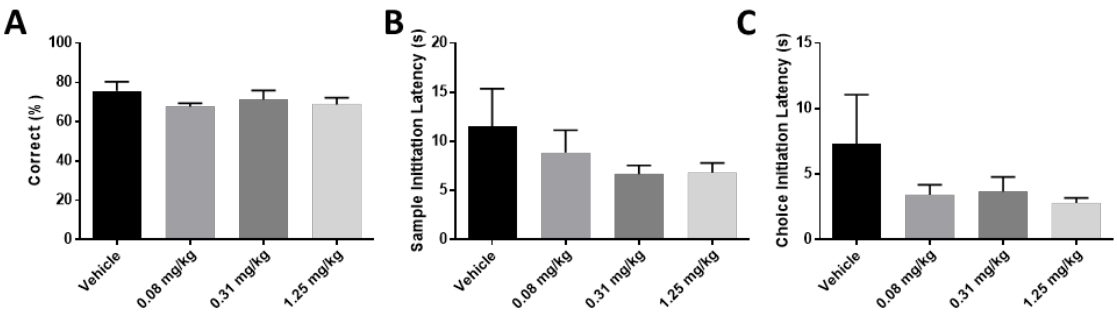

Figure S2. *Lower doses of RO 25-6981 did not cause a significant change in working memory performance, sample initiation latency or choice initiation latency* **A.** Lower doses of RO 25-6981 (0.08 mg/kg, 0.31 mg/kg, 1.25 mg/kg) treatment did not cause any significant change in working memory performance (n = 8, $F_{(1.66, 11.62)} = 1.219$, $P = 0.0598$). **B.** Sample initiation latencies were comparable after treatment with lower doses of RO 25-6981 (n = 8, $F_{(1.516, 10.61)} = 1.23$, $P = 0.3171$) **C.** Choice latencies were comparable after treatment with lower doses of RO 25-6981 (n = 8, $F_{(1.606, 11,24)} = 1.327$, $P = 0.2959$). Values show group mean ± SEM.

Fig. S3

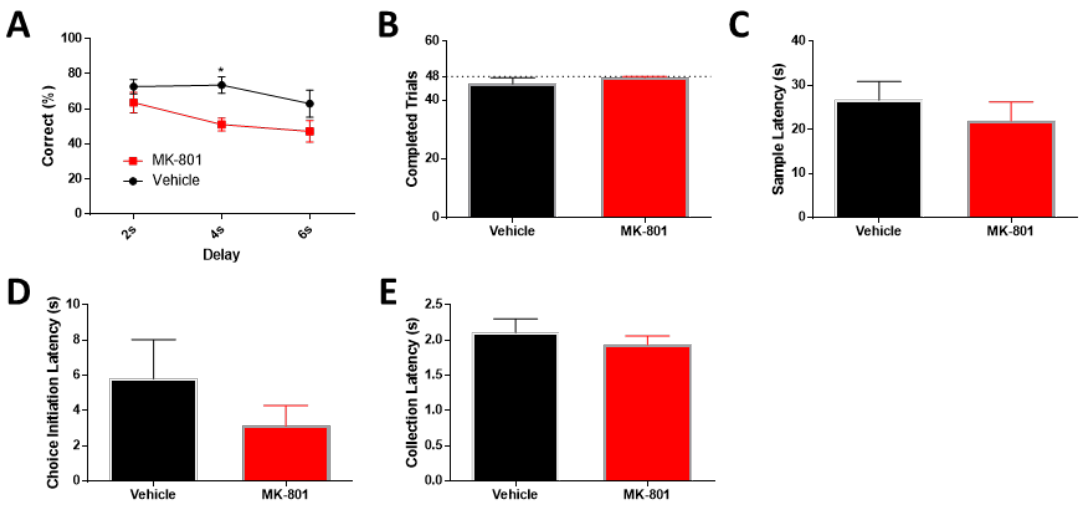

Figure S3. *Detailed analyses of TUNL parameters after MK-801 treatment.* **A.** Delay-dependent impairment was enhanced after MK-801 treatment ($F_{(2, 28)} = 4$, $P = 0.0296$ for effect of delay, $F_{(1, 14)} = 7.473$, $P = 0.0162$ for effect of drug, $P_{adj} = 0.5838$ for 2 s, $P_{adj} = 0.0193$ for 4 s, $P_{adj} = 0.1455$ for 6 s). **B.** There was no significant effect of MK-801 treatment on number of completed trials (n = 8, $P = 0.3628$). Maximum number of trials was limited to 48. **C.** There was no significant effect of MK-801 treatment on sample latency (n = 8, $P = 0.3594$) **D.** There was no significant effect of MK-801 treatment on choice initiation latency (n = 8, $P = 0.3111$) **E.** There was no significant effect of MK-801 treatment on collection latency (n = 8, $P = 0.1482$) Values show group mean ± SEM.; $^*P < 0.05$.

Fig. S4

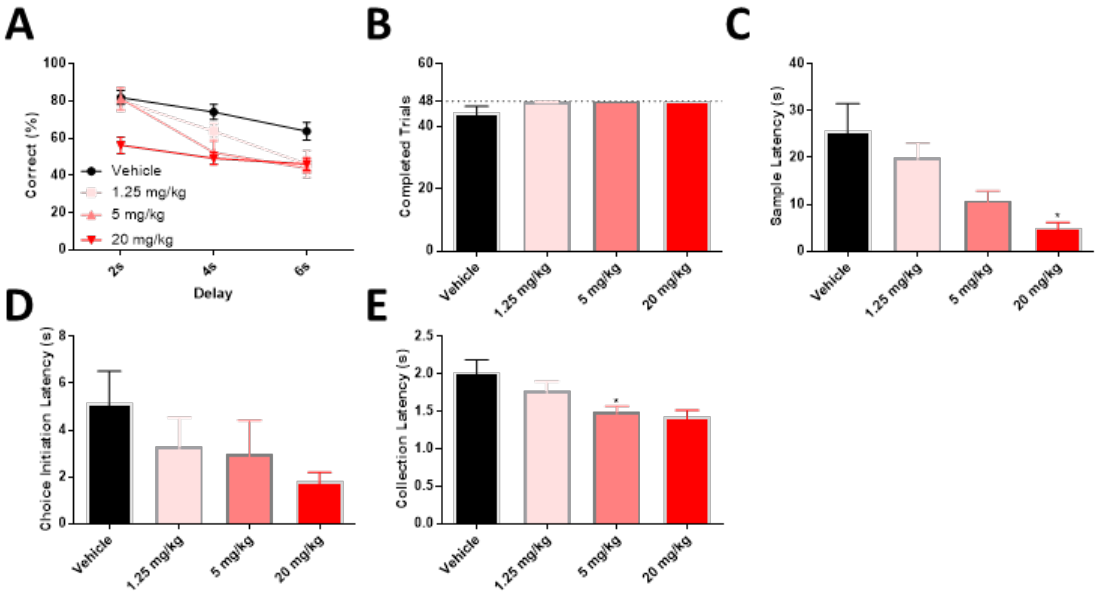

Figure S4. *Detailed analyses of TUNL parameters after RO 25-6981 treatment.* **A.** There was a significant delay-dependent and RO 25-6981-induced impairment ($F_{(2, 56)} = 31.54$, $P < 0.0001$ for effect of delay, $F_{(3, 28)} = 9.048$, $P = 0.0002$ for effect of drug; For 2 s delay: $P_{adj} > 0.9999$ for 1.25 mg/kg, $P_{adj} > 0.9999$ for 5 mg/kg, $P_{adj} = 0.0029$ for 20 mg/kg; For 4 s delay: $P_{adj} = 0.7237$ for 1.25 mg/kg, $P_{adj} = 0.0176$ for 5 mg/kg, $P_{adj} = 0.0040$ for 20 mg/kg; For 6 s delay: $P_{adj} = 0.0972$ for 1.25 mg/kg, $P_{adj} = 0.0382$ for 5 mg/kg, $P_{adj} = 0.0972$ for 20 mg/kg). **B.** There was no significant effect of RO 25-6981 treatment on number of completed trials (n = 8, $F_{(1.033, 7.233)} = 3.416$, $P = 0.1051$). Maximum number of trials was limited to 48. **C.** There was a significant effect of RO 25-6981 treatment on sample latency (n = 8, $F_{(1.411, 9.879)} = 7.843$, $P = 0.0135$, $P_{adj} = 0.7271$ for 1.25 mg/kg, $P_{adj} = 0.0874$ for 5 mg/kg, $P_{adj} = 0.0256$ for 20 mg/kg). **D.** There was no significant effect of RO 25-6981 treatment on choice initiation latency (n = 8, $F_{(1.613, 11.29)} = 3.131$, $P = 0.0902$). **E.** There was a significant effect of RO 25-6981 treatment on collection latency (n = 8, $F_{(1.382, 9.677)} = 8.321$, $P = 0.0120$,

$P_{adj} = 0.0833$ for 1.25 mg/kg, $P_{adj} = 0.0166$ for 5 mg/kg, $P_{adj} = 0.0546$ for 20 mg/kg). Values show group mean $\pm$ SEM.; n.s.: $p \geq 0.05$, $^{*}P < 0.05$.

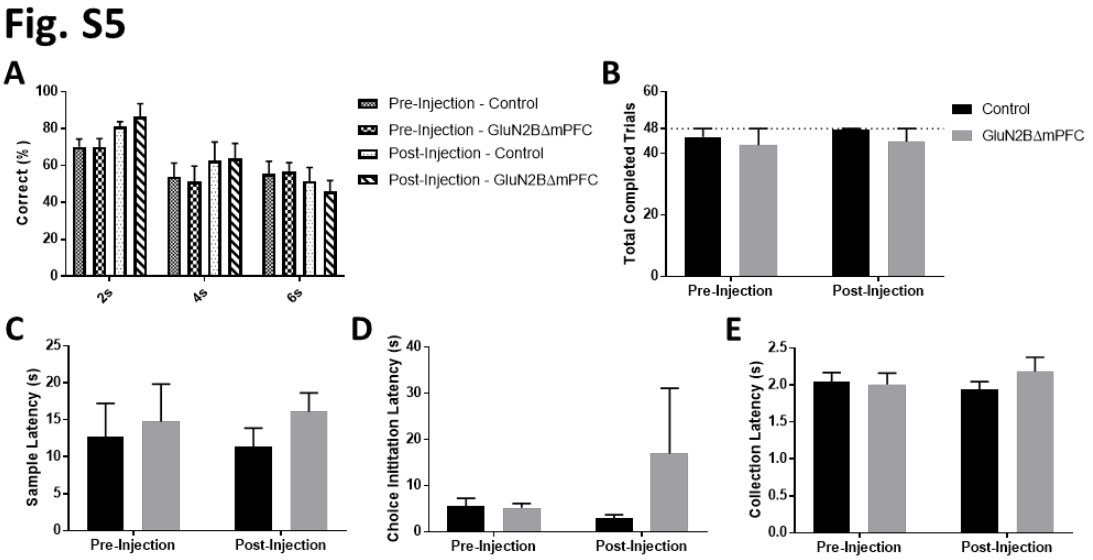

Figure S5. *GluN2B deletion in mPFC did not cause any significant changes in TUNL parameters analyzed* **A.** There was a significant delay-dependent worsening in working memory performance but no change after viral injection ($F_{(2, 36)} = 15.01$, $P < 0.0001$ for delay, $F_{(3, 18)} = 0.5785$, $P = 0.6366$ for viral injection). **B.** There was no significant effect of GluN2B deletion in mPFC on number of completed trials ($F_{(1, 9)} = 0.4738$, $P = 0.5086$ for virus type, $F_{(1, 9)} = 1.64$, $P = 0.2323$ for injection status). Maximum number of trials was limited to 48. **C.** There was no significant effect of GluN2B deletion in mPFC on sample latency ($F_{(1, 9)} = 0.4893$, $P = 0.5019$ for virus type, $F_{(1, 9)} = 0.0006$, $P = 0.9810$ for injection status) **D.** There was no significant effect of GluN2B deletion in mPFC on choice initiation latency ($F_{(1, 9)} = 1.027$, $P = 0.3373$ for virus type, $F_{(1, 9)} = 0.5211$, $P = 0.4887$ for injection status) **E.** There was no significant effect of GluN2B deletion in mPFC on collection latency ($F_{(1, 9)} = 0.2845$, $P = 0.6067$ for virus type, $F_{(1, 9)} = 0.2428$, $P = 0.6340$ for injection status) Values show group mean $\pm$ SEM.

Fig. S6

A

In Absence of Cre:

Co-expression of EGFP and mCherry but no siRNA.

In Presence of Cre:

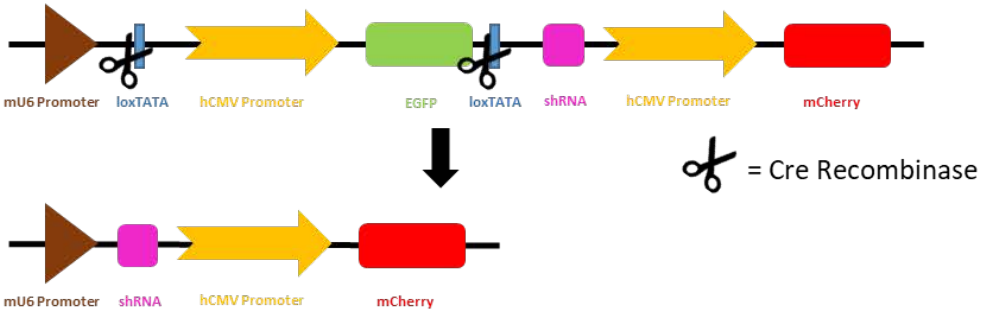

mCherry expression together with siRNA, no EGFP.

B

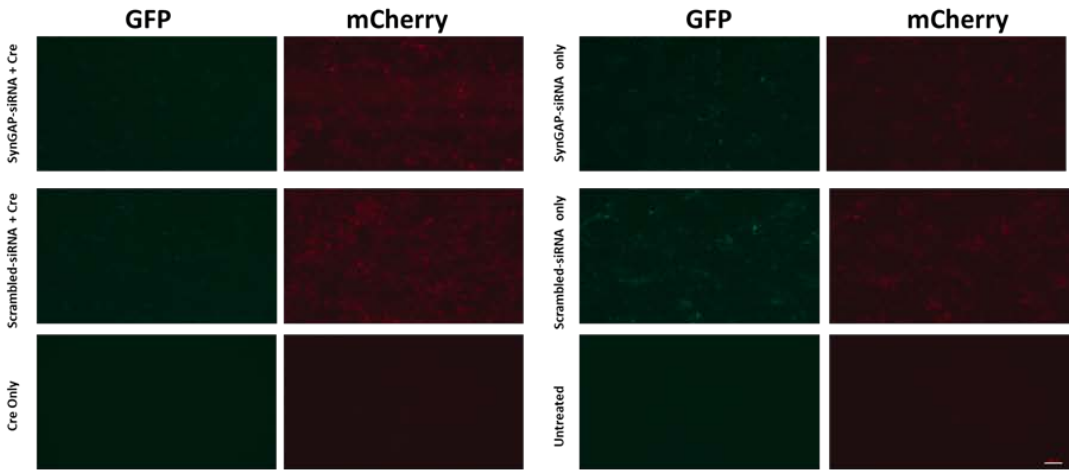

C

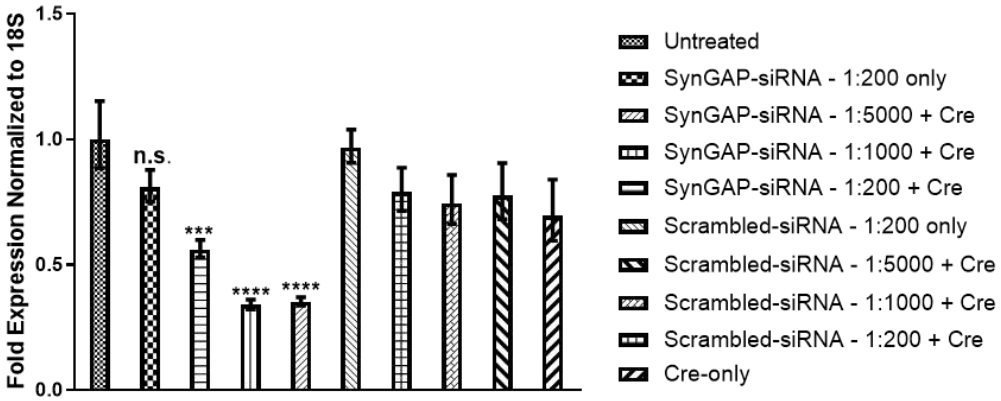

Figure S6. *Design and characterization of conditional AAV virus for Syngap1 knockdown* **A.** Simplified schematic of the viral vector we designed for shRNA expression in a Cre-dependent manner. In absence of Cre recombinase, murine U6 promoter is spatially separated from shRNA cassette by EGFP positioned between two loxTATA boxes. Therefore, activity of U6 promoter is suppressed and RNA Polymerase III cannot have access to shRNA cassette for siRNA synthesis. In absence of Cre recombinase, EGFP and mCherry are co-expressed but no siRNA can be synthesized. In presence of Cre recombinase, upstream hCMV promoter and EGFP sequence are incised completely from loxTATA sites, which results in U6 promoter and shRNA cassette coming into close vicinity. Therefore, RNA Polymerase III can have access to U6 promoter and shRNA, and synthesize siRNA. In presence of Cre recombinase, EGFP can no longer be synthesized but mCherry and shRNA can be transcribed. **B.** Fluorescent imaging of primary neuronal cultures that were transduced with SynGAP-siRNA and Scrambled-siRNA viruses confirmed reduction of GFP signal in co-presence of Cre recombinase (upper and middle panel, compare GFP columns; reduced GFP expression in the left panel in presence of Cre compared to the right panel in absence of Cre). mCherry expression was also enhanced both for SynGAP-siRNA and Scrambled-siRNA viruses in presence of Cre (upper and middle panel, compare mCherry columns; enhanced mCherry expression in the left panel in presence of Cre compared to the right panel in absence of Cre). Cre-only or untreated conditions did not yield any GFP or mCherry expression. **C.** RT-qPCR analysis revealed a highly significant and dose-dependent knockdown of *Syngap1* after co-transduction of SynGAP-siRNA virus and Cre (Ordinary one-way ANOVA, $F_{(4, 20)} = 35.44$, $P < 0.0001$, $P_{adj} = 0.2304$ for 1:200 only, $P_{adj} = 0.0003$ for 1:5000 + Cre, $P_{adj} < 0.0001$ for 1:1000 + Cre, $P_{adj} < 0.0001$ for 1:200 + Cre). There was no significant change in *Syngap1* levels after co-transduction of the Scrambled-siRNA virus and Cre (Ordinary one-way ANOVA, $F_{(4, 20)} = 1.304$, $P = 0.3023$). Cre transduction-only did not yield any significant change in *Syngap1* levels compared to Untreated group (Unpaired t

test, n = 5 biological replicates, $P = 0.1311$). Values show group mean ± SEM.; ***$P < 0.001$, ****$P < 0.0001$. Scale bar represents 100 μm.

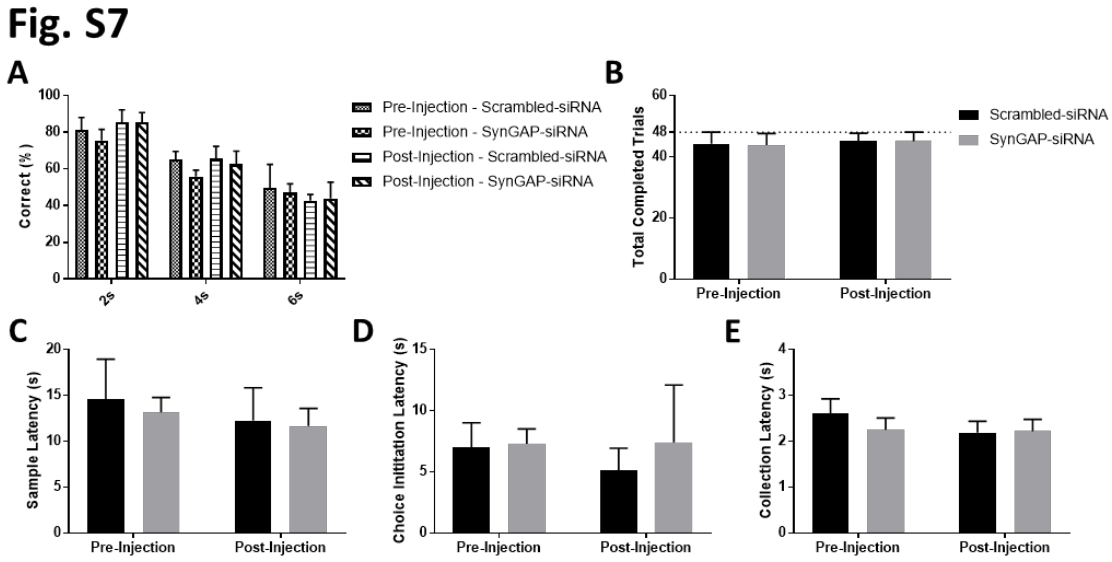

Figure S7. *Syngap1 knockdown in mPFC did not cause any significant changes in TUNL parameters analyzed* **A.** There was a significant delay-dependent worsening in working memory performance but no change after viral injection ($F_{(2, 32)} = 36.05$, $P < 0.0001$ for delay, $F_{(3, 16)} = 0.3517$, $P = 0.7885$ for viral injection). **B.** There was no significant effect of *Syngap1* knockdown in mPFC on number of completed trials ($F_{(1, 8)} = 0.003194$, $P = 0.9563$ for virus type, $F_{(1, 8)} = 0.00386$, $P = 0.9520$ for injection status). Maximum number of trials was limited to 48. **C.** There was no significant effect of *Syngap1* knockdown in mPFC on sample latency ($F_{(1, 8)} = 0.09682$, $P = 0.7636$ for virus type, $F_{(1, 8)} = 0.04987$, $P = 0.8289$ for injection status) **D.** There was no significant effect of *Syngap1* knockdown in mPFC on choice initiation latency ($F_{(1, 8)} = 0.1632$, $P = 0.6968$ for virus type, $F_{(1, 8)} = 0.07337$, $P = 0.7934$ for injection status) **E.** There was no significant effect of *Syngap1* knockdown in mPFC on collection latency ($F_{(1, 8)} = 0.1821$, $P = 0.6808$ for virus type, $F_{(1, 8)} = 2.993$, $P = 0.1219$ for injection status) Values show group mean $\pm$ SEM.

Supplementary Materials and Methods

Primary Cortical Culture and Viral Transduction

Primary cortical culture was prepared as previously described (47). Plating concentration of neuronal culture was 1 x 10^6 cell/ml. Cultures were transduced on DIV 7-9 by directly adding diluted viral particles in sterile PBS and incubated for 4-6 days. For Cre expression in cortical cultures, CAV2-CMV-Cre from the Center National de la Recherche Scientifique (203) was used with a final dilution of 1:200. SynGAP-siRNA targeted 19 bp sequence of GCCATAGAAGAGTATATGA while Scrambled-siRNA sequence was GGTGGATAATCGTAACAAA.

Immunohistochemistry

For validation of injection sites, mice were transcardially perfused with 4% PFA in PBS. Brains were post-fixed in 4% PFA overnight at 4°C and then transferred to PBS until sectioning. Brains were sliced into 50 µM free-floating coronal sections using a vibratome (VT1000 S, Leica Biosystems, Nussloch, Germany). Sections were washed 3 times for 10 minutes with PBS containing 0.5% Triton-X-100 (PBST). After blocking for 2 h at room temperature with PBST containing 5% normal horse serum (NHS). Slices were incubated in PBST containing 2.5% NHS overnight at 4°C with primary antibody. Slices were washed 3 times for 10 minutes in PBST and incubated with secondary antibody diluted to 1:2000 in PBST containing 2.5% NHS for 2 hours at room temperature. Slices were washed 3 times for 10 minutes in PBS. In second wash, DAPI with a working concentration of 5 µg/ml (Cat# 40043, Biotium, Inc., Fremont, CA, USA) was added for nucleic acid staining. Slices were mounted with ProLong™ Gold Antifade Mountant (P10144, Thermo Fisher Scientific, Waltham, MA, USA). Primary antibodies and working concentrations are as follows: Anti-Cre recombinase (mouse monoclonal, 1:400, Sigma, Cat#MAB3120), Anti-GFP (chicken polyclonal, 1:1000, Cat#A10262, Thermo Fisher Scientific), Anti-DsRed (for mCherry

staining, rabbit polyclonal, 1:1000, Cat#632496, Clontech), Anti-GluN2B (mouse monoclonal, 1:400, Cat#75-097, NeuroMab), GluN2B (rabbit polyclonal, 1:400, Cat#TA328822, OriGene). Sections were imaged using an inverted microscope (Axio Vert.A1, ZEISS, Oberkochen, Germany).

RNA Isolation and RT-qPCR

Total RNA was isolated using Qiagen® RNeasy® Mini Kit (Hilden, Germany) according to manufacturer's protocol. Optional DNase treatment step was performed. One-step RT-qPCR was performed using AgPath-ID™ One-Step RT-PCR kit (Cat# 4387391, Thermo Fisher Scientific) according to recommended protocol with a Roche LightCycler® 480 Instrument (Roche Molecular Systems, Inc., Pleasanton, CA, USA). TaqMan probes (Thermo Fisher Scientific) were used to detect *Syngap1* (Assay ID Mm01306150_m1) and 18S rRNA levels (Assay ID Hs99999901_s1). C_t values were calculated using absolute quantification/2nd derivative maximum method in high confidence mode with LightCycler® 480 Software, Version 1.5. The Comparative C_T Method (also referred as the $\Delta\Delta C_T$ Method) was used to calculate relative *Syngap1* expression levels normalized to 18S rRNA levels and untreated sample. Standard deviation values of $\Delta\Delta C_T$ were used for statistical analysis. $\Delta\Delta C_T$ and SEM values were incorporated into fold-difference.

Concluding Remarks and Future Outlook

Despite the increasing interest in and continuing research, elucidating spatial and temporal expression patterns of lncRNAs is still necessary for understanding their dynamics in the nervous system and neurodevelopmental disorders (93). To address this need, we performed an RNA-Seq study and demonstrated that some ASD-related genes and their antisense transcripts are differentially expressed between mPFC and striatum through development. These differences should be taken into account in order to obtain a more comprehensive understanding of the interplay of sense-antisense partners that lead to the disease state. The differentially expresses genes from the analysis should be studied more in depth to understand their circuit specific roles and involvement in neurological mechanisms that lead to pathology.

In general, a comprehensive mouse antisense transcriptome with tissue and developmental age specific annotations for mouse brain is lacking. In this thesis, *de novo* antisense transcriptome with over 70,000 contigs for the mPFC and striatum was generated to partially fulfill this need. This novel antisense transcriptome can be used as a reference for determining NAT candidates for research activities in the CNS and its disorders. However, the functional confirmation of the identified transcripts is still an essential requirement for any subsequent study.

In this thesis, the blast analysis of *de novo* antisense transcripts identified highly complementary and covered sequences between mouse and human. This finding is particularly important for generating preclinical models to study lncRNA function in relation to CNS diseases. However, it should be noted that sequence homology is not the

only factor that determines functional similarity in different species and a more comprehensive approach is necessary to draw conclusions (187).

Given that our study is contributing to the understanding of lncRNA research, epidemiological studies carried out on patients and further development in bioinformatics are crucial to have a better understanding of the lncRNA function in general and to gain a better insight into their roles in ASD and other neurodevelopmental diseases (93, 204, 205).

In this thesis, working memory assay TUNL was optimized for pharmacological testing in mice. This approach can be further improved and applied to study biological mechanisms and distinct modalities of cognition, and to develop and test therapeutics for the CNS diseases. Nevertheless, the limitations of animal studies for studying human-specific neurodevelopmental conditions should always be taken into consideration should these findings are translated to humans.

As demonstrated in this thesis, the glutamatergic system has an important role in regulating cognitive related processes. Therefore, targeting glutamatergic signaling using NMDAR modulators stands out as a promising modality for the treatment of cognitive disturbances seen in patients with neurodevelopmental diseases. Functional brain network understanding of how glutamatergic compounds are affecting cognition could contribute to the potential success of glutamatergic drug validation (122).

References

1. American Psychiatric Association., American Psychiatric Association. DSM-5 Task Force. Diagnostic and statistical manual of mental disorders : DSM-5. 5th ed. Washington, D.C.: American Psychiatric Association; 2013. xliv, 947 p. p.

2. Christensen DL, Baio J, Van Naarden Braun K, Bilder D, Charles J, Constantino JN, et al. Prevalence and Characteristics of Autism Spectrum Disorder Among Children Aged 8 Years--Autism and Developmental Disabilities Monitoring Network, 11 Sites, United States, 2012. MMWR Surveill Summ. 2016;65(3):1-23.

3. Risch N, Hoffmann TJ, Anderson M, Croen LA, Grether JK, Windham GC. Familial Recurrence of Autism Spectrum Disorder: Evaluating Genetic and Environmental Contributions. American Journal of Psychiatry. 2014;171(11):1206-13.

4. Geschwind DH. Advances in autism. Annu Rev Med. 2009;60:367-80.

5. Ramaswami G, Geschwind DH. Genetics of autism spectrum disorder. Neurogenetics, Part I. Handbook of Clinical Neurology2018. p. 321-9.

6. Aldinger KA, Lane CJ, Veenstra-VanderWeele J, Levitt P. Patterns of Risk for Multiple Co-Occurring Medical Conditions Replicate Across Distinct Cohorts of Children with Autism Spectrum Disorder. Autism Res. 2015;8(6):771-81.

7. Baron-Cohen S. The cognitive neuroscience of autism. J Neurol Neurosurg Psychiatry. 2004;75(7):945-8.

8. Hempel CM, Sugino K, Nelson SB. A manual method for the purification of fluorescently labeled neurons from the mammalian brain. Nat Protoc. 2007;2(11):2924-9.

9. Ameis SH, Catani M. Altered white matter connectivity as a neural substrate for social impairment in Autism Spectrum Disorder. Cortex. 2015;62:158-81.

10. Dajani DR, Uddin LQ. Local brain connectivity across development in autism spectrum disorder: A cross-sectional investigation. Autism Research. 2016;9(1):43-54.

11. Courchesne E, Mouton PR, Calhoun ME, Semendeferi K, Ahrens-Barbeau C, Hallet MJ, et al. Neuron number and size in prefrontal cortex of children with autism. JAMA. 2011;306(18):2001-10.

12. Stoner R, Chow ML, Boyle MP, Sunkin SM, Mouton PR, Roy S, et al. Patches of disorganization in the neocortex of children with autism. N Engl J Med. 2014;370(13):1209-19.

13. Donovan AP, Basson MA. The neuroanatomy of autism - a developmental perspective. J Anat. 2017;230(1):4-15.

14. Chow ML, Pramparo T, Winn ME, Barnes CC, Li HR, Weiss L, et al. Age-dependent brain gene expression and copy number anomalies in autism suggest distinct pathological processes at young versus mature ages. PLoS Genet. 2012;8(3):e1002592.

15. Rothwell PE. Autism Spectrum Disorders and Drug Addiction: Common Pathways, Common Molecules, Distinct Disorders? Frontiers in Neuroscience. 2016;10.

16. Dölen G, Sahin M. Editorial: Essential Pathways and Circuits of Autism Pathogenesis. Frontiers in Neuroscience. 2016;10.

17. Fuccillo MV. Striatal Circuits as a Common Node for Autism Pathophysiology. Front Neurosci. 2016;10:27.

18. Colvert E, Tick B, McEwen F, Stewart C, Curran SR, Woodhouse E, et al. Heritability of Autism Spectrum Disorder in a UK Population-Based Twin Sample. JAMA Psychiatry. 2015;72(5):415-23.

19. Tick B, Bolton P, Happe F, Rutter M, Rijsdijk F. Heritability of autism spectrum disorders: a meta-analysis of twin studies. J Child Psychol Psychiatry. 2016;57(5):585-95.

20. Gronborg TK, Schendel DE, Parner ET. Recurrence of autism spectrum disorders in full- and half-siblings and trends over time: a population-based cohort study. JAMA Pediatr. 2013;167(10):947-53.

21. Gaugler T, Klei L, Sanders SJ, Bodea CA, Goldberg AP, Lee AB, et al. Most genetic risk for autism resides with common variation. Nat Genet. 2014;46(8):881-5.

22. Quesnel-Vallieres M, Weatheritt RJ, Cordes SP, Blencowe BJ. Autism spectrum disorder: insights into convergent mechanisms from transcriptomics. Nat Rev Genet. 2019;20(1):51-63.

23. Ronemus M, Iossifov I, Levy D, Wigler M. The role of de novo mutations in the genetics of autism spectrum disorders. Nat Rev Genet. 2014;15(2):133-41.

24. Abrahams BS, Arking DE, Campbell DB, Mefford HC, Morrow EM, Weiss LA, et al. SFARI Gene 2.0: a community-driven knowledgebase for the autism spectrum disorders (ASDs). Molecular Autism. 2013;4.

25. Geschwind DH. Autism: many genes, common pathways? Cell. 2008;135(3):391-5.

26. Betancur C. Etiological heterogeneity in autism spectrum disorders: More than 100 genetic and genomic disorders and still counting. Brain research. 2011;1380:42-77.

27. Pinto D, Delaby E, Merico D, Barbosa M, Merikangas A, Klei L, et al. Convergence of Genes and Cellular Pathways Dysregulated in Autism Spectrum Disorders. Am J Hum Genet. 2014;94(5):677-94.

28. Sanders SJ, Xin H, Willsey AJ, Ercan-Sencicek AG, Samocha KE, Cicek AE, et al. Insights into Autism Spectrum Disorder Genomic Architecture and Biology from 71 Risk Loci. Neuron. 2015;87(6):1215-33.

29. Geschwind DH, State MW. Gene hunting in autism spectrum disorder: on the path to precision medicine. Lancet Neurol. 2015;14(11):1109-20.

30. Gandal MJ, Haney JR, Parikshak NN, Leppa V, Ramaswami G, Hartl C, et al. Shared molecular neuropathology across major psychiatric disorders parallels polygenic overlap. Science. 2018;359(6376):693-7.

31. Traynelis SF, Wollmuth LP, McBain CJ, Menniti FS, Vance KM, Ogden KK, et al. Glutamate receptor ion channels: structure, regulation, and function. Pharmacol Rev. 2010;62(3):405-96.

32. Cooke SF. Plasticity in the human central nervous system. Brain. 2006;129(7):1659-73.

33. Paoletti P, Bellone C, Zhou Q. NMDA receptor subunit diversity: impact on receptor properties, synaptic plasticity and disease. Nat Rev Neurosci. 2013;14(6):383-400.

34. Paoletti P. Molecular basis of NMDA receptor functional diversity. Eur J Neurosci. 2011;33(8):1351-65.

35. Cull-Candy SG, Leszkiewicz DN. Role of distinct NMDA receptor subtypes at central synapses. Sci STKE. 2004;2004(255):re16.

36. Gladding CM, Raymond LA. Mechanisms underlying NMDA receptor synaptic/extrasynaptic distribution and function. Mol Cell Neurosci. 2011;48(4):308-20.

37. Paoletti P, Neyton J. NMDA receptor subunits: function and pharmacology. Curr Opin Pharmacol. 2007;7(1):39-47.

38. Wang CC, Held RG, Chang SC, Yang L, Delpire E, Ghosh A, et al. A critical role for GluN2B-containing NMDA receptors in cortical development and function. Neuron. 2011;72(5):789-805.

39. Gray JA, Shi Y, Usui H, During MJ, Sakimura K, Nicoll RA. Distinct modes of AMPA receptor suppression at developing synapses by GluN2A and GluN2B: single-cell NMDA receptor subunit deletion in vivo. Neuron. 2011;71(6):1085-101.

40. Naassila M, Pierrefiche O. GluN2B Subunit of the NMDA Receptor: The Keystone of the Effects of Alcohol During Neurodevelopment. Neurochemical research. 2019;44(1):78-88.

41. Thomas CG, Miller AJ, Westbrook GL. Synaptic and extrasynaptic NMDA receptor NR2 subunits in cultured hippocampal neurons. Journal of neurophysiology. 2006;95(3):1727-34.

42. Vicini S, Wang JF, Li JH, Zhu WJ, Wang YH, Luo JH, et al. Functional and pharmacological differences between recombinant N-methyl-D-aspartate receptors. Journal of neurophysiology. 1998;79(2):555-66.

43. Lau CG, Zukin RS. NMDA receptor trafficking in synaptic plasticity and neuropsychiatric disorders. Nat Rev Neurosci. 2007;8(6):413-26.

44. Tovar KR, Westbrook GL. Mobile NMDA receptors at hippocampal synapses. Neuron. 2002;34(2):255-64.

45. Groc L, Heine M, Cousins SL, Stephenson FA, Lounis B, Cognet L, et al. NMDA receptor surface mobility depends on NR2A-2B subunits. Proc Natl Acad Sci U S A. 2006;103(49):18769-74.

46. Sun YJ, Xu YG, Cheng XK, Chen X, Xie YH, Zhang LA, et al. The differences between GluN2A and GluN2B signaling in the brain. J Neurosci Res. 2018;96(8):1430-43.

47. Hall BJ, Ripley B, Ghosh A. NR2B signaling regulates the development of synaptic AMPA receptor current. J Neurosci. 2007;27(49):13446-56.

48. Barria A, Malinow R. NMDA receptor subunit composition controls synaptic plasticity by regulating binding to CaMKII. Neuron. 2005;48(2):289-301.

49. Leonard AS, Lim IA, Hemsworth DE, Horne MC, Hell JW. Calcium/calmodulin-dependent protein kinase II is associated with the N-methyl-D-aspartate receptor. Proc Natl Acad Sci U S A. 1999;96(6):3239-44.

50. Wang CC, Held RG, Hall BJ. SynGAP regulates protein synthesis and homeostatic synaptic plasticity in developing cortical networks. PLoS One. 2013;8(12):e83941.

51. Chen HJ, Rojas-Soto M, Oguni A, Kennedy MB. A synaptic Ras-GTPase activating protein (p135 SynGAP) inhibited by CaM kinase II. Neuron. 1998;20(5):895-904.

52. Kim JH, Liao DZ, Lau LF, Huganir RL. SynGAP: a synaptic RasGAP that associates with the PSD-95/SAP90 protein family. Neuron. 1998;20(4):683-91.

53. Krapivinsky G, Medina I, Krapivinsky L, Gapon S, Clapham DE. SynGAP-MUPP1-CaMKII synaptic complexes regulate p38 MAP kinase activity and NMDA receptor-dependent synaptic AMPA receptor potentiation. Neuron. 2004;43(4):563-74.

54. Pena V, Hothorn M, Eberth A, Kaschau N, Parret A, Gremer L, et al. The C2 domain of SynGAP is essential for stimulation of the Rap GTPase reaction. EMBO Rep. 2008;9(4):350-5.

55. Walkup WGt, Washburn L, Sweredoski MJ, Carlisle HJ, Graham RL, Hess S, et al. Phosphorylation of synaptic GTPase-activating protein (synGAP) by Ca2+/calmodulin-dependent protein kinase II (CaMKII) and cyclin-dependent kinase 5 (CDK5) alters the ratio of its GAP activity toward Ras and Rap GTPases. The Journal of biological chemistry. 2015;290(8):4908-27.

56. Vazquez LE, Chen HJ, Sokolova I, Knuesel I, Kennedy MB. SynGAP regulates spine formation. J Neurosci. 2004;24(40):8862-72.

57. Kim MJ, Dunah AW, Wang YT, Sheng M. Differential roles of NR2A- and NR2B-containing NMDA receptors in Ras-ERK signaling and AMPA receptor trafficking. Neuron. 2005;46(5):745-60.

58. Clement JP, Aceti M, Creson TK, Ozkan ED, Shi Y, Reish NJ, et al. Pathogenic SYNGAP1 mutations impair cognitive development by disrupting maturation of dendritic spine synapses. Cell. 2012;151(4):709-23.

59. Clement JP, Ozkan ED, Aceti M, Miller CA, Rumbaugh G. SYNGAP1 links the maturation rate of excitatory synapses to the duration of critical-period synaptic plasticity. J Neurosci. 2013;33(25):10447-52.

60. Holder JL, Jr., Hamdan FF, Michaud JL. SYNGAP1-Related Intellectual Disability. In: Adam MP, Ardinger HH, Pagon RA, Wallace SE, Bean LJH, Stephens K, et al., editors. GeneReviews((R)). Seattle (WA)1993.

61. Hamdan FF, Gauthier J, Spiegelman D, Noreau A, Yang Y, Pellerin S, et al. Mutations in SYNGAP1 in autosomal nonsyndromic mental retardation. N Engl J Med. 2009;360(6):599-605.

62. Berryer MH, Hamdan FF, Klitten LL, Moller RS, Carmant L, Schwartzentruber J, et al. Mutations in SYNGAP1 cause intellectual disability, autism, and a specific form of epilepsy by inducing haploinsufficiency. Hum Mutat. 2013;34(2):385-94.

63. Velmeshev D, Magistri M, Faghihi MA. Expression of non-protein-coding antisense RNAs in genomic regions related to autism spectrum disorders. Mol Autism. 2013;4(1):32.

64. Davis CA, Hitz BC, Sloan CA, Chan ET, Davidson JM, Gabdank I, et al. The Encyclopedia of DNA elements (ENCODE): data portal update. Nucleic Acids Research. 2018;46(D1):D794-D801.

65. Consortium EP. The ENCODE (ENCyclopedia Of DNA Elements) Project. Science. 2004;306(5696):636-40.

66. Consortium EP. An integrated encyclopedia of DNA elements in the human genome. Nature. 2012;489(7414):57-74.

67. Derrien T, Johnson R, Bussotti G, Tanzer A, Djebali S, Tilgner H, et al. The GENCODE v7 catalog of human long noncoding RNAs: analysis of their gene structure, evolution, and expression. Genome Res. 2012;22(9):1775-89.

68. Harrow J, Frankish A, Gonzalez JM, Tapanari E, Diekhans M, Kokocinski F, et al. GENCODE: the reference human genome annotation for The ENCODE Project. Genome Res. 2012;22(9):1760-74.

69. Katayama S, Tomaru Y, Kasukawa T, Waki K, Nakanishi M, Nakamura M, et al. Antisense transcription in the mammalian transcriptome. Science. 2005;309(5740):1564-6.

70. Carninci P, Kasukawa T, Katayama S, Gough J, Frith MC, Maeda N, et al. The transcriptional landscape of the mammalian genome. Science. 2005;309(5740):1559-63.

71. Derrien T, Guigo R, Johnson R. The Long Non-Coding RNAs: A New (P)layer in the "Dark Matter". Front Genet. 2011;2:107.

72. He Z, Bammann H, Han D, Xie G, Khaitovich P. Conserved expression of lincRNA during human and macaque prefrontal cortex development and maturation. RNA. 2014;20(7):1103-11.

73. Necsulea A, Soumillon M, Warnefors M, Liechti A, Daish T, Zeller U, et al. The evolution of lncRNA repertoires and expression patterns in tetrapods. Nature. 2014;505(7485):635-40.

74. Cuevas-Diaz Duran R, Wei H, Kim DH, Wu JQ. Review: Long non-coding RNAs: important regulators in the development, function and disorders of the central nervous system. Neuropathol Appl Neurobiol. 2019.

75. Kung JT, Colognori D, Lee JT. Long noncoding RNAs: past, present, and future. Genetics. 2013;193(3):651-69.

76. Ponjavic J, Ponting CP, Lunter G. Functionality or transcriptional noise? Evidence for selection within long noncoding RNAs. Genome Res. 2007;17(5):556-65.

77. Kapranov P, Willingham AT, Gingeras TR. Genome-wide transcription and the implications for genomic organization. Nat Rev Genet. 2007;8(6):413-23.

78. Duran RC, Yan H, Zheng Y, Huang X, Grill R, Kim DH, et al. The systematic analysis of coding and long non-coding RNAs in the sub-chronic and chronic stages of spinal cord injury. Sci Rep. 2017;7:41008.

79. Cabili MN, Trapnell C, Goff L, Koziol M, Tazon-Vega B, Regev A, et al. Integrative annotation of human large intergenic noncoding RNAs reveals global properties and specific subclasses. Genes & development. 2011;25(18):1915-27.

80. Guttman M, Amit I, Garber M, French C, Lin MF, Feldser D, et al. Chromatin signature reveals over a thousand highly conserved large non-coding RNAs in mammals. Nature. 2009;458(7235):223-7.

81. Mercer TR, Dinger ME, Sunkin SM, Mehler MF, Mattick JS. Specific expression of long noncoding RNAs in the mouse brain. Proc Natl Acad Sci U S A. 2008;105(2):716-21.

82. Hu W, Alvarez-Dominguez JR, Lodish HF. Regulation of mammalian cell differentiation by long non-coding RNAs. EMBO Rep. 2012;13(11):971-83.

83. Rasool M, Malik A, Zahid S, Basit Ashraf MA, Qazi MH, Asif M, et al. Non-coding RNAs in cancer diagnosis and therapy. Noncoding RNA Res. 2016;1(1):69-76.

84. Militello G, Weirick T, John D, Doring C, Dimmeler S, Uchida S. Screening and validation of lncRNAs and circRNAs as miRNA sponges. Brief Bioinform. 2017;18(5):780-8.

85. Gaiti F, Fernandez-Valverde SL, Nakanishi N, Calcino AD, Yanai I, Tanurdzic M, et al. Dynamic and Widespread lncRNA Expression in a Sponge and the Origin of Animal Complexity. Mol Biol Evol. 2015;32(9):2367-82.

86. Ng SY, Johnson R, Stanton LW. Human long non-coding RNAs promote pluripotency and neuronal differentiation by association with chromatin modifiers and transcription factors. EMBO J. 2012;31(3):522-33.

87. Tsai MC, Manor O, Wan Y, Mosammaparast N, Wang JK, Lan F, et al. Long Noncoding RNA as Modular Scaffold of Histone Modification Complexes. Science. 2010;329(5992):689-93.

88. Gong C, Maquat LE. lncRNAs transactivate STAU1-mediated mRNA decay by duplexing with 3' UTRs via Alu elements. Nature. 2011;470(7333):284-8.

89. Tripathi V, Ellis JD, Shen Z, Song DY, Pan Q, Watt AT, et al. The nuclear-retained noncoding RNA MALAT1 regulates alternative splicing by modulating SR splicing factor phosphorylation. Mol Cell. 2010;39(6):925-38.

90. van de V, II, Gordebeke PM, Khoshab N, Tiesinga PH, Buitelaar JK, Kozicz T, et al. Long non-coding RNAs in neurodevelopmental disorders. Front Mol Neurosci. 2013;6:53.

91. Hamosh A, Scott AF, Amberger JS, Bocchini CA, McKusick VA. Online Mendelian Inheritance in Man (OMIM), a knowledgebase of human genes and genetic disorders. Nucleic Acids Res. 2005;33(Database issue):D514-7.

92. van Bokhoven H. Genetic and epigenetic networks in intellectual disabilities. Annu Rev Genet. 2011;45:81-104.

93. Tang J, Yu Y, Yang W. Long noncoding RNA and its contribution to autism spectrum disorders. CNS Neurosci Ther. 2017;23(8):645-56.

94. Parikshak NN, Swarup V, Belgard TG, Irimia M, Ramaswami G, Gandal MJ, et al. Genome-wide changes in lncRNA, splicing, and regional gene expression patterns in autism. Nature. 2016;540(7633):423-7.

95. Ziats MN, Rennert OM. Aberrant expression of long noncoding RNAs in autistic brain. J Mol Neurosci. 2013;49(3):589-93.

96. Wang K, Zhang H, Ma D, Bucan M, Glessner JT, Abrahams BS, et al. Common genetic variants on 5p14.1 associate with autism spectrum disorders. Nature. 2009;459(7246):528-33.

97. Khorkova O, Hsiao J, Wahlestedt C. Oligonucleotides for upregulating gene expression. Pharm Pat Anal. 2013;2(2):215-29.

98. Khorkova O, Wahlestedt C. Oligonucleotide therapies for disorders of the nervous system. Nat Biotechnol. 2017;35(3):249-63.

99. Khorkova O, Myers AJ, Hsiao J, Wahlestedt C. Natural antisense transcripts. Hum Mol Genet. 2014;23(R1):R54-63.

100. Halley P, Khorkova O, Wahlestedt C. Natural antisense transcripts as therapeutic targets. Drug Discov Today Ther Strateg. 2013;10(3):e119-e25.

101. Wahlestedt C. Natural antisense and noncoding RNA transcripts as potential drug targets. Drug Discov Today. 2006;11(11-12):503-8.

102. Modarresi F, Faghihi MA, Lopez-Toledano MA, Fatemi RP, Magistri M, Brothers SP, et al. Inhibition of natural antisense transcripts in vivo results in gene-specific transcriptional upregulation. Nat Biotechnol. 2012;30(5):453-9.

103. Pennington BF, Ozonoff S. Executive functions and developmental psychopathology. J Child Psychol Psychiatry. 1996;37(1):51-87.

104. Scheurich A. Handbook of neuropsychological tests: attention, memory and executive functions. Verhaltenstherapie. 2010;20(2):143-4.

105. Goldstein S, Naglieri JA. Handbook of executive functioning. New York, NY: Springer; 2014. xix, 567 p. p.

106. Toichi M, Kamio Y. Long-term memory and levels-of-processing in autism. Neuropsychologia. 2002;40(7):964-9.

107. Hvoslef-Eide M, Nilsson SRO, Saksida LM, Bussey TJ. Cognitive Translation Using the Rodent Touchscreen Testing Approach. Translational Neuropsychopharmacology. Current Topics in Behavioral Neurosciences2015. p. 423-47.

108. Insel TR. Next-generation treatments for mental disorders. Sci Transl Med. 2012;4(155):155ps19.

109. Sahakian BJ, Owen AM. Computerized Assessment in Neuropsychiatry Using Cantab - Discussion Paper. J Roy Soc Med. 1992;85(7):399-402.

110. Levaux MN, Potvin S, Sepehry AA, Sablier J, Mendrek A, Stip E. Computerized assessment of cognition in schizophrenia: Promises and pitfalls of CANTAB. Eur Psychiat. 2007;22(2):104-15.

111. Barnett JH, Robbins TW, Leeson VC, Sahakian BJ, Joyce EM, Blackwell AD. Assessing cognitive function in clinical trials of schizophrenia. Neurosci Biobehav R. 2010;34(8):1161-77.

112. Talpos JC, McTighe SM, Dias R, Saksida LM, Bussey TJ. Trial-unique, delayed nonmatching-to-location (TUNL): a novel, highly hippocampus-dependent automated touchscreen test of location memory and pattern separation. Neurobiol Learn Mem. 2010;94(3):341-52.

113. Oomen CA, Hvoslef-Eide M, Heath CJ, Mar AC, Horner AE, Bussey TJ, et al. The touchscreen operant platform for testing working memory and pattern separation in rats and mice. Nat Protoc. 2013;8(10):2006-21.

114. Cowan N. Working Memory Underpins Cognitive Development, Learning, and Education. Educ Psychol Rev. 2014;26(2):197-223.

115. McCarthy G, Blamire AM, Puce A, Nobre AC, Bloch G, Hyder F, et al. Functional magnetic resonance imaging of human prefrontal cortex activation during a spatial working memory task. Proc Natl Acad Sci U S A. 1994;91(18):8690-4.

116. Galloway EM, Woo NH, Lu B. Persistent neural activity in the prefrontal cortex: a mechanism by which BDNF regulates working memory? Prog Brain Res. 2008;169:251-66.

117. Dudchenko PA. An overview of the tasks used to test working memory in rodents. Neuroscience & Biobehavioral Reviews. 2004;28(7):699-709.

118. Bussey TJ, Holmes A, Lyon L, Mar AC, McAllister KAL, Nithianantharajah J, et al. New translational assays for preclinical modelling of cognition in schizophrenia: The touchscreen testing method for mice and rats. Neuropharmacology. 2012;62(3):1191-203.

119. Horner AE, Heath CJ, Hvoslef-Eide M, Kent BA, Kim CH, Nilsson SR, et al. The touchscreen operant platform for testing learning and memory in rats and mice. Nat Protoc. 2013;8(10):1961-84.

120. McAllister KA, Saksida LM, Bussey TJ. Dissociation between memory retention across a delay and pattern separation following medial prefrontal cortex lesions in the touchscreen TUNL task. Neurobiol Learn Mem. 2013;101:120-6.

121. Kim CH, Romberg C, Hvoslef-Eide M, Oomen CA, Mar AC, Heath CJ, et al. Trial-unique, delayed nonmatching-to-location (TUNL) touchscreen testing for mice: sensitivity to dorsal hippocampal dysfunction. Psychopharmacology (Berl). 2015;232(21-22):3935-45.

122. Dauvermann MR, Lee G, Dawson N. Glutamatergic regulation of cognition and functional brain connectivity: insights from pharmacological, genetic and translational schizophrenia research. British Journal of Pharmacology. 2017;174(19):3136-60.

123. de Bruin NM, van Drimmelen M, Kops M, van Elk J, Wetering MM, Schwienbacher I. Effects of risperidone, clozapine and the 5-HT6 antagonist GSK-742457 on PCP-induced deficits in reversal learning in the two-lever operant task in male Sprague Dawley rats. Behav Brain Res. 2013;244:15-28.

124. Gastambide F, Mitchell SN, Robbins TW, Tricklebank MD, Gilmour G. Temporally distinct cognitive effects following acute administration of ketamine and phencyclidine in the rat. Eur Neuropsychopharmacol. 2013;23(11):1414-22.

125. Amitai N, Markou A. Effects of metabotropic glutamate receptor 2/3 agonism and antagonism on schizophrenia-like cognitive deficits induced by phencyclidine in rats. Eur J Pharmacol. 2010;639(1-3):67-80.

126. Barnes SA, Young JW, Bate ST, Neill JC. Dopamine D1 receptor activation improves PCP-induced performance disruption in the 5C-CPT by reducing inappropriate responding. Behav Brain Res. 2016;300:45-55.

127. Thomson DM, McVie A, Morris BJ, Pratt JA. Dissociation of acute and chronic intermittent phencyclidine-induced performance deficits in the 5-choice serial reaction time task: influence of clozapine. Psychopharmacology (Berl). 2011;213(4):681-95.

128. Noda Y, Kamei H, Mamiya T, Furukawa H, Nabeshima T. Repeated phencyclidine treatment induces negative symptom-like behavior in forced swimming test in mice: imbalance of prefrontal serotonergic and dopaminergic functions. Neuropsychopharmacology. 2000;23(4):375-87.

129. Kumar G, Olley J, Steckler T, Talpos J. Dissociable effects of NR2A and NR2B NMDA receptor antagonism on cognitive flexibility but not pattern separation. Psychopharmacology (Berl). 2015;232(21-22):3991-4003.

130. Hurtubise JL, Marks WN, Davies DA, Catton JK, Baker GB, Howland JG. MK-801-induced impairments on the trial-unique, delayed nonmatching-to-location task in rats: effects of acute sodium nitroprusside. Psychopharmacology (Berl). 2017;234(2):211-22.

131. Cadinu D, Grayson B, Podda G, Harte MK, Doostdar N, Neill JC. NMDA receptor antagonist rodent models for cognition in schizophrenia and identification of novel drug treatments, an update. Neuropharmacology. 2018;142:41-62.

132. von Engelhardt J, Doganci B, Jensen V, Hvalby O, Gongrich C, Taylor A, et al. Contribution of hippocampal and extra-hippocampal NR2B-containing NMDA receptors to performance on spatial learning tasks. Neuron. 2008;60(5):846-60.

133. Brigman JL, Daut RA, Wright T, Gunduz-Cinar O, Graybeal C, Davis MI, et al. GluN2B in corticostriatal circuits governs choice learning and choice shifting. Nat Neurosci. 2013;16(8):1101-10.

134. Marquardt K, Josey M, Kenton JA, Cavanagh JF, Holmes A, Brigman JL. Impaired cognitive flexibility following NMDAR-GluN2B deletion is associated with altered orbitofrontal-striatal function. Neuroscience. 2019;404:338-52.

135. Miller OH, Yang L, Wang CC, Hargroder EA, Zhang Y, Delpire E, et al. GluN2B-containing NMDA receptors regulate depression-like behavior and are critical for the rapid antidepressant actions of ketamine. Elife. 2014;3:e03581.

136. Guo X, Hamilton PJ, Reish NJ, Sweatt JD, Miller CA, Rumbaugh G. Reduced expression of the NMDA receptor-interacting protein SynGAP causes behavioral abnormalities that model symptoms of Schizophrenia. Neuropsychopharmacology. 2009;34(7):1659-72.

137. Muhia M, Feldon J, Knuesel I, Yee BK. Appetitively motivated instrumental learning in SynGAP heterozygous knockout mice. Behav Neurosci. 2009;123(5):1114-28.

138. Muhia M, Yee BK, Feldon J, Markopoulos F, Knuesel I. Disruption of hippocampus-regulated behavioural and cognitive processes by heterozygous constitutive deletion of SynGAP. Eur J Neurosci. 2010;31(3):529-43.

139. Muhia M, Willadt S, Yee BK, Feldon J, Paterna JC, Schwendener S, et al. Molecular and behavioral changes associated with adult hippocampus-specific SynGAP1 knockout. Learn Mem. 2012;19(7):268-81.

140. Berryer MH, Chattopadhyaya B, Xing P, Riebe I, Bosoi C, Sanon N, et al. Decrease of SYNGAP1 in GABAergic cells impairs inhibitory synapse connectivity, synaptic inhibition and cognitive function. Nat Commun. 2016;7:13340.

141. Ozkan ED, Creson TK, Kramar EA, Rojas C, Seese RR, Babyan AH, et al. Reduced cognition in Syngap1 mutants is caused by isolated damage within developing forebrain excitatory neurons. Neuron. 2014;82(6):1317-33.

142. Komiyama NH, Watabe AM, Carlisle HJ, Porter K, Charlesworth P, Monti J, et al. SynGAP regulates ERK/MAPK signaling, synaptic plasticity, and learning in the complex with postsynaptic density 95 and NMDA receptor. J Neurosci. 2002;22(22):9721-32.

143. Deacon RM, Rawlins JN. T-maze alternation in the rodent. Nat Protoc. 2006;1(1):7-12.

144. Elsabbagh M, Divan G, Koh Y-J, Kim YS, Kauchali S, Marcín C, et al. Global Prevalence of Autism and Other Pervasive Developmental Disorders. Autism Research. 2012;5(3):160-79.

145. Amaral DG, Schumann CM, Nordahl CW. Neuroanatomy of autism. Trends Neurosci. 2008;31(3):137-45.

146. Quan Z, Zheng D, Qing H. Regulatory Roles of Long Non-Coding RNAs in the Central Nervous System and Associated Neurodegenerative Diseases. Front Cell Neurosci. 2017;11:175.

147. Elling R, Chan J, Fitzgerald KA. Emerging role of long noncoding RNAs as regulators of innate immune cell development and inflammatory gene expression. Eur J Immunol. 2016;46(3):504-12.

148. Briggs JA, Wolvetang EJ, Mattick JS, Rinn JL, Barry G. Mechanisms of Long Non-coding RNAs in Mammalian Nervous System Development, Plasticity, Disease, and Evolution. Neuron. 2015;88(5):861-77.

149. Magistri M, Faghihi MA, St Laurent G, 3rd, Wahlestedt C. Regulation of chromatin structure by long noncoding RNAs: focus on natural antisense transcripts. Trends Genet. 2012;28(8):389-96.

150. Chen J, Sun M, Hurst LD, Carmichael GG, Rowley JD. Genome-wide analysis of coordinate expression and evolution of human cis-encoded sense-antisense transcripts. Trends Genet. 2005;21(6):326-9.

151. Qureshi IA, Mattick JS, Mehler MF. Long non-coding RNAs in nervous system function and disease. Brain research. 2010;1338:20-35.

152. Esteller M. Non-coding RNAs in human disease. Nat Rev Genet. 2011;12(12):861-74.

153. Qureshi IA, Mehler MF. Long non-coding RNAs: novel targets for nervous system disease diagnosis and therapy. Neurotherapeutics. 2013;10(4):632-46.

154. Roberts TC, Morris KV, Wood MJ. The role of long non-coding RNAs in neurodevelopment, brain function and neurological disease. Philos Trans R Soc Lond B Biol Sci. 2014;369(1652).

155. Barry G. Integrating the roles of long and small non-coding RNA in brain function and disease. Mol Psychiatry. 2014;19(4):410-6.

156. Merelo V, Durand D, Lescallette AR, Vrana KE, Hong LE, Faghihi MA, et al. Associating schizophrenia, long non-coding RNAs and neurostructural dynamics. Front Mol Neurosci. 2015;8:57.

157. Meng L, Ward AJ, Chun S, Bennett CF, Beaudet AL, Rigo F. Towards a therapy for Angelman syndrome by targeting a long non-coding RNA. Nature. 2015;518(7539):409-12.

158. Cogill SB, Srivastava AK, Yang MQ, Wang L. Co-expression of long non-coding RNAs and autism risk genes in the developing human brain. BMC Syst Biol. 2018;12(Suppl 7):91.

159. Spijker S. Dissection of Rodent Brain Regions. Neuroproteomics. Neuromethods2011. p. 13-26.

160. Wu TD, Watanabe CK. GMAP: a genomic mapping and alignment program for mRNA and EST sequences. Bioinformatics. 2005;21(9):1859-75.

161. Wu TD, Nacu S. Fast and SNP-tolerant detection of complex variants and splicing in short reads. Bioinformatics. 2010;26(7):873-81.

162. Li H, Handsaker B, Wysoker A, Fennell T, Ruan J, Homer N, et al. The Sequence Alignment/Map format and SAMtools. Bioinformatics. 2009;25(16):2078-9.

163. Mortazavi A, Williams BA, McCue K, Schaeffer L, Wold B. Mapping and quantifying mammalian transcriptomes by RNA-Seq. Nat Methods. 2008;5(7):621-8.

164. Dobin A, Davis CA, Schlesinger F, Drenkow J, Zaleski C, Jha S, et al. STAR: ultrafast universal RNA-seq aligner. Bioinformatics. 2013;29(1):15-21.

165. Grabherr MG, Haas BJ, Yassour M, Levin JZ, Thompson DA, Amit I, et al. Full-length transcriptome assembly from RNA-Seq data without a reference genome. Nature Biotechnology. 2011;29(7):644-52.

166. Haas BJ, Papanicolaou A, Yassour M, Grabherr M, Blood PD, Bowden J, et al. De novo transcript sequence reconstruction from RNA-seq using the Trinity platform for reference generation and analysis. Nature Protocols. 2013;8(8):1494-512.

167. Love MI, Huber W, Anders S. Moderated estimation of fold change and dispersion for RNA-seq data with DESeq2. Genome Biology. 2014;15(12).

168. Robinson MD, McCarthy DJ, Smyth GK. edgeR: a Bioconductor package for differential expression analysis of digital gene expression data. Bioinformatics. 2010;26(1):139-40.

169. McCarthy DJ, Chen Y, Smyth GK. Differential expression analysis of multifactor RNA-Seq experiments with respect to biological variation. Nucleic Acids Res. 2012;40(10):4288-97.

170. Dillman AA, Cookson MR. Transcriptomic Changes in Brain Development. Brain Transcriptome. International Review of Neurobiology2014. p. 233-50.

171. Christakis DA, Ramirez JSB, Ferguson SM, Ravinder S, Ramirez J-M. How early media exposure may affect cognitive function: A review of results from observations in humans and experiments in mice. Proceedings of the National Academy of Sciences. 2018;115(40):9851-8.

172. Thierry-Mieg D, Thierry-Mieg J. AceView: a comprehensive cDNA-supported gene and transcripts annotation. Genome Biol. 2006;7 Suppl 1:S12 1-4.

173. Chamberlain SJ, Brannan CI. The Prader–Willi Syndrome Imprinting Center Activates the Paternally Expressed Murine Ube3a Antisense Transcript but Represses Paternal Ube3a. Genomics. 2001;73(3):316-22.

174. Mills JD, Kawahara Y, Janitz M. Strand-Specific RNA-Seq Provides Greater Resolution of Transcriptome Profiling. Curr Genomics. 2013;14(3):173-81.

175. Zhao W, He X, Hoadley KA, Parker JS, Hayes D, Perou CM. Comparison of RNA-Seq by poly (A) capture, ribosomal RNA depletion, and DNA microarray for expression profiling. BMC Genomics. 2014;15(1).

176. Cabili MN, Dunagin MC, McClanahan PD, Biaesch A, Padovan-Merhar O, Regev A, et al. Localization and abundance analysis of human lncRNAs at single-cell and single-molecule resolution. Genome Biol. 2015;16:20.

177. Faghihi MA, Modarresi F, Khalil AM, Wood DE, Sahagan BG, Morgan TE, et al. Expression of a noncoding RNA is elevated in Alzheimer's disease and drives rapid feed-forward regulation of beta-secretase. Nat Med. 2008;14(7):723-30.

178. Araujo DJ, Anderson AG, Berto S, Runnels W, Harper M, Ammanuel S, et al. FoxP1 orchestration of ASD-relevant signaling pathways in the striatum. Genes & development. 2015;29(20):2081-96.

179. Francis F, Koulakoff A, Boucher D, Chafey P, Schaar B, Vinet MC, et al. Doublecortin is a developmentally regulated, microtubule-associated protein expressed in migrating and differentiating neurons. Neuron. 1999;23(2):247-56.

180. Vourc'h P, Petit E, Muh JP, Andres C, Bienvenu T, Beldjord C, et al. Exclusion of the coding sequence of the doublecortin gene as a susceptibility locus in autistic disorder. Am J Med Genet. 2002;108(2):164-7.

181. Reiner O, Coquelle FM, Peter B, Levy T, Kaplan A, Sapir T, et al. The evolving doublecortin (DCX) superfamily. BMC Genomics. 2006;7:188.

182. Uesaka M, Nishimura O, Go Y, Nakashima K, Agata K, Imamura T. Bidirectional promoters are the major source of gene activation-associated non-coding RNAs in mammals. Bmc Genomics. 2014;15.

183. Batagov AO, Yarmishyn AA, Jenjaroenpun P, Tan JZ, Nishida Y, Kurochkin IV. Role of genomic architecture in the expression dynamics of long noncoding RNAs during differentiation of human neuroblastoma cells. BMC Syst Biol. 2013;7 Suppl 3:S11.

184. Hsiao J, Yuan TY, Tsai MS, Lu CY, Lin YC, Lee ML, et al. Upregulation of Haploinsufficient Gene Expression in the Brain by Targeting a Long Non-coding RNA Improves Seizure Phenotype in a Model of Dravet Syndrome. EBioMedicine. 2016;9:257-77.

185. Faghihi MA, Kocerha J, Modarresi F, Engstrom PG, Chalk AM, Brothers SP, et al. RNAi screen indicates widespread biological function for human natural antisense transcripts. PLoS One. 2010;5(10).

186. Mitchell AC, Javidfar B, Pothula V, Ibi D, Shen EY, Peter CJ, et al. MEF2C transcription factor is associated with the genetic and epigenetic risk architecture of schizophrenia and improves cognition in mice. Molecular Psychiatry. 2017;23(1):123-32.

187. Mathews DH, Moss WN, Turner DH. Folding and finding RNA secondary structure. Cold Spring Harb Perspect Biol. 2010;2(12):a003665.

188. Dingledine R, Borges K, Bowie D, Traynelis SF. The glutamate receptor ion channels. Pharmacol Rev. 1999;51(1):7-61.

189. Moretto E, Murru L, Martano G, Sassone J, Passafaro M. Glutamatergic synapses in neurodevelopmental disorders. Progress in Neuro-Psychopharmacology and Biological Psychiatry. 2018;84:328-42.

190. Funk AJ, McCullumsmith RE, Haroutunian V, Meador-Woodruff JH. Abnormal activity of the MAPK- and cAMP-associated signaling pathways in frontal cortical areas in postmortem brain in schizophrenia. Neuropsychopharmacology. 2012;37(4):896-905.

191. Euston DR, Gruber AJ, McNaughton BL. The Role of Medial Prefrontal Cortex in Memory and Decision Making. Neuron. 2012;76(6):1057-70.

192. Schmitt LI, Wimmer RD, Nakajima M, Happ M, Mofakham S, Halassa MM. Thalamic amplification of cortical connectivity sustains attentional control. Nature. 2017;545(7653):219-23.

193. Bolkan SS, Stujenske JM, Parnaudeau S, Spellman TJ, Rauffenbart C, Abbas AI, et al. Thalamic projections sustain prefrontal activity during working memory maintenance. Nat Neurosci. 2017;20(7):987-96.

194. Miller OH, Bruns A, Ben Ammar I, Mueggler T, Hall BJ. Synaptic Regulation of a Thalamocortical Circuit Controls Depression-Related Behavior. Cell Rep. 2017;20(8):1867-80.

195. Ventura A, Meissner A, Dillon CP, McManus M, Sharp PA, Van Parijs L, et al. Cre-lox-regulated conditional RNA interference from transgenes. Proceedings of the National Academy of Sciences of the United States of America. 2004;101(28):10380-5.

196. Gorski JA, Talley T, Qiu M, Puelles L, Rubenstein JL, Jones KR. Cortical excitatory neurons and glia, but not GABAergic neurons, are produced in the Emx1-expressing lineage. J Neurosci. 2002;22(15):6309-14.

197. Franklin KBJ, Paxinos G. Paxinos and Franklin's The mouse brain in stereotaxic coordinates. Fourth edition. ed. Amsterdam: Academic Press, an imprint of Elsevier; 2013. 1 volume (unpaged) p.

198. Lein ES, Hawrylycz MJ, Ao N, Ayres M, Bensinger A, Bernard A, et al. Genome-wide atlas of gene expression in the adult mouse brain. Nature. 2007;445(7124):168-76.

199. Dudchenko PA, Talpos J, Young J, Baxter MG. Animal models of working memory: a review of tasks that might be used in screening drug treatments for the memory impairments found in schizophrenia. Neurosci Biobehav Rev. 2013;37(9 Pt B):2111-24.

200. Zarate CA, Singh JB, Carlson PJ, Brutsche NE, Ameli R, Luckenbaugh DA, et al. A Randomized Trial of an N-methyl-D-aspartate Antagonist in Treatment-Resistant Major Depression. Archives of General Psychiatry. 2006;63(8).

201. Watson TD, Petrakis IL, Edgecombe J, Perrino A, Krystal JH, Mathalon DH. Modulation of the cortical processing of novel and target stimuli by drugs affecting glutamate and GABA neurotransmission. Int J Neuropsychopharmacol. 2009;12(3):357-70.

202. Spellman T, Rigotti M, Ahmari SE, Fusi S, Gogos JA, Gordon JA. Hippocampal-prefrontal input supports spatial encoding in working memory. Nature. 2015;522(7556):309-14.

203. Soudais C, Laplace-Builhe C, Kissa K, Kremer EJ. Preferential transduction of neurons by canine adenovirus vectors and their efficient retrograde transport in vivo. FASEB J. 2001;15(12):2283-5.

204. Guo X, Gao L, Wang Y, Chiu DK, Wang T, Deng Y. Advances in long noncoding RNAs: identification, structure prediction and function annotation. Brief Funct Genomics. 2016;15(1):38-46.

205. Luo H, Bu D, Sun L, Fang S, Liu Z, Zhao Y. Identification and function annotation of long intervening noncoding RNAs. Brief Bioinform. 2017;18(5):789-97.